





RESEARCH ARTICLE | AUGUST 08 2024

Radiation in the black hole–plasma system: Propagation in equatorial plane

Vladimír Balek   ; Barbora Bezděková  ; Jiří Bičák 



J. Math. Phys. 65, 082501 (2024)

<https://doi.org/10.1063/5.0200901>



Articles You May Be Interested In

Toroidal LNRF-velocity profiles in thick accretion discs orbiting rapidly rotating Kerr black holes

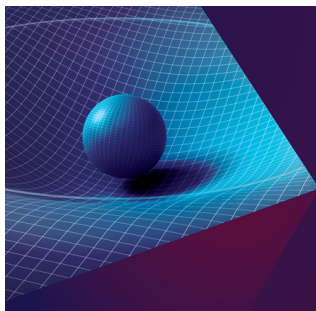
AIP Conference Proceedings (November 2006)

Formulating the equation of relativistic mass accretion rate for extreme Kerr black holes with accretion disk on the equatorial plane

AIP Conf. Proc. (May 2020)

Relativistic mass rates of accreted matter with accretion discs in the equatorial plane of slowly rotating neutron stars

AIP Conf. Proc. (May 2023)



Journal of Mathematical Physics

Special Topics Open for Submissions

[Learn More](#)

Radiation in the black hole–plasma system: Propagation in equatorial plane

Cite as: J. Math. Phys. 65, 082501 (2024); doi: 10.1063/5.0200901

Submitted: 29 January 2024 • Accepted: 16 July 2024 •

Published Online: 8 August 2024



View Online



Export Citation



CrossMark

Vladimír Balek,^{1,a)}  Barbora Bezděková,²  and Jiří Bičák^{2,b)} 

AFFILIATIONS

¹Department of Theoretical Physics, Comenius University, Bratislava, Slovakia

²Institute of Theoretical Physics, Charles University, Prague, Czech Republic

^{a)} Author to whom correspondence should be addressed: balek@fmph.uniba.sk

^{b)} Deceased.

ABSTRACT

Effect of cold plasma on the form of rays propagating in the equatorial plane of a rotating black hole is investigated. Two kinds of regions in the radius–impact parameter plane allowed for the rays are constructed: for radiation with a given frequency at infinity and for radiation with a given “telescope frequency” seen by a local observer. The form of allowed regions for locally nonrotating observers as well as observers falling freely from infinity is established. The allowed regions contain rays which directly reach the horizon, or there exists a “neck” connecting the forbidden regions such that the rays coming from infinity cannot reach the horizon. In case we considered a set of observers at various radii instead of the neck we find two different regions – from one the rays reach the horizon and not infinity and from the other one they reach infinity, but not the horizon. The results are analyzed by analytical methods and illustrated by figures constructed numerically.

Published under an exclusive license by AIP Publishing. <https://doi.org/10.1063/5.0200901>

I. INTRODUCTION

It is widely acknowledged that in 1911 Albert Einstein, in his best known paper written during his Prague stay, addressed the question of the influence of gravity on light (“Über den Einfluß der Schwerkraft auf die Ausbreitung des Lichtes”) and suggested that the bending of rays moving close to the Sun should be observable. Less is known that Einstein had derived the lens equation, predicted the double images and the magnifications in the year 1912, as documented in his notebook written during his visit of Berlin from Prague.¹ As a consequence of many significant developments in both theory and observations, the effects of gravity on the light propagation have become subject of numerous studies. For very comprehensive reviews on gravitational lensing, see, for example, Refs. 2–5.

In the following we do not address directly gravitational lensing, rather, we turn to more general question about the existence of allowed regions for rays propagating in the gravitational field of a rotating (Kerr) black hole which is surrounded by a cold plasma.

Let us first mention works on light rays in the fields of black holes in vacuum. The pioneering study of the allowed regions for both photons and free massive particles around a Kerr black hole in the equatorial plane were done many years ago by De Felice.⁶ He determined and analyzed the turning points in terms of impact parameter, and constructed also diagrams corresponding to various particle energies and black hole angular momenta. Allowed regions in lensing problems around a Kerr black hole in vacuum were more recently discussed, e.g., by Vazquez and Esteban⁷ and Gralla and Lupsasca.⁸ The values of impact (“critical”) parameter for which circular light rays exist were derived by Iyer and Hansen.⁹ Their paper also includes the study of ray deflection angles, proving that there is the light bending asymmetry due to hole’s rotation.

For related works on the photon escape cones from black hole’s vicinity, see Refs. 10–12 and a new comprehensive review by Ogasawara and Igata.¹³

Only recently the light ray trajectories in Kerr spacetime were studied assuming also the presence of a medium in the spacetime (see, e.g., Refs. 14–16 and references therein).

In the present paper, we study the allowed regions for rays in cold plasma in the vicinity of a Kerr black hole. Our basic parameters to characterize the rays are the impact parameter at infinity and the frequency of radiation. In case of the frequency we distinguish two physically distinct situations: either the frequency ω is fixed at infinity, or we consider a given “telescope frequency” ω_0 which is fixed by the requirement that it is measured by a given observer located outside the horizon.

Unlike in the study of De Felice,⁶ we investigate the turning points for rays around a Kerr black hole surrounded by a refractive and dispersive medium in geometrical optics approximation by using the elegant Hamiltonian formalism by Synge.¹⁷ This formalism was employed in developing the radiation transfer theory in refractive and dispersive media in curved spacetimes by Bičák and Hadrava,¹⁸ for example, and it has been used recently in a number of studies to describe ray behavior in refractive and dispersive media in the vicinity of black holes. The focus is usually on gravitational lensing, on black hole shadow etc. Let us mention just few examples. In the series of papers by Bisnovatyi-Kogan and Tsupko, e.g., Refs. 19–22, the authors found the deflection angle formulas in dispersive media around a Schwarzschild black hole. The form of the shadow of a Kerr black hole surrounded by plasma was derived by Perlick and Tsupko¹⁴ and further investigated by Chowdhuri and Bhattacharyya.¹⁶ Fathi *et al.*¹⁵ used the separability condition for the Hamilton–Jacobi equation from Ref. 14, assumed some simple ansatz for the radial and longitudinal dependence of plasma frequency, and calculated the light rays analytically in terms of elliptic integrals. More generally, separability of the Hamilton–Jacobi equation and shadow in axially symmetric spacetimes with plasma was recently analyzed in Ref. 23.

The dispersion of light rays around a Kerr black hole caused by the presence of a plasma with a power distributed density was studied by Kimpson *et al.*²⁴ Sárený and Balek²⁵ investigated light rays in several models of plasma in the vicinity of a Kerr black hole.

In our work, we employ the distribution of nonsingular isothermal sphere²⁶ for plasma. The distribution of a (non)singular isothermal sphere lies somewhere between exponential and power-law distributions used as density models for spiral and elliptical galaxies, respectively.²⁷ It is frequently used in the description of gravitational lensing by galaxies or clusters of galaxies.²⁸ In such studies, the inhomogeneity parameter in the plasma distribution is by many orders of magnitude greater than the size of a typical black hole in the center of galaxy. We will be interested in the effect of plasma on the propagation of radiation in close proximity of the black hole, therefore we will suppose the parameter to be of the same order as the radius of the horizon. Note that in an accretion disc consisting of hot plasma,²⁹ the distribution of plasma in the outer region, where the radiative transfer of energy is dominated by free-free transitions, is similar to the distribution inside a nonsingular sphere far from the black hole (density of plasma is proportional to r^{-2} in the nonsingular sphere, and approximately proportional to $r^{-15/8}$ in the disc).

In the following section the Hamiltonian method for rays in a curved spacetime with a (non-gravitating) medium described by a space-time dependent and frequency dependent index of refraction n is introduced. The medium is then considered to be a cold non-magnetic plasma characterized by the electron density N_e and plasma frequency ω_{pl} . In order to determine regions to which the light rays can propagate, we have to make sure that (i) the Hamilton equations are satisfied, and (ii) the constraint of the vanishing Hamiltonian is fulfilled. The latter condition guarantees that the index of refraction remains real along any given ray. The conditions are specified in the Kerr metric. The frequency of the radiation as seen by a general observer is expressed, in particular for the observers locally non-rotating (LNRF) and for observers freely falling from the rest from infinity.

In Sec. III allowed regions for the radiation with the fixed frequency as measured at infinity are analyzed in detail in analytic terms, and specific examples are constructed numerically. First the vacuum case is considered, then plasma is added. As could be anticipated, the forbidden regions are larger than in vacuum. This is well seen in the diagrams showing the radial coordinate a ray can reach when having given impact parameter and frequency at infinity. Frequency can, of course, be negative as seen at infinity if a ray is close to the horizon and cannot reach infinity. We pay a particular attention to the formation of “necks” in the radius and impact parameters plane which connect forbidden regions.

In Sec. IV a detailed analysis is devoted to the illustration of the allowed regions when a ray should reach a given LNRF observer with a given frequency ω_0 . In Appendixes A–D we give more detailed discussion of the formation of the neck in both cases when ω or ω_0 are fixed, we investigate the allowed regions far/near to infinity, and provide the analysis of the allowed regions when LNRF observer’s position and the impact parameter are given.

In Sec. V and Appendix E the allowed regions are analyzed for observers freely falling from the rest at infinity. Again, both analytical and graphical and numerical results are presented. We give detailed explanations of the results by combining both analytical considerations and number of figures constructed numerically. One can concentrate primarily on the introductions to each section and on the figure captions if one does not wish to follow detailed “analytical” argumentations.

We use the system of units $c = G = 1$ and the signature of the metric $(- + + +)$.

II. ALLOWED REGIONS FOR RADIATION IN A MEDIUM IN KERR SPACETIME

Consider an electromagnetic wave propagating in a refractive and dispersive medium with refractive index n in flat spacetime. Denote the frequency and the wave vector of the wave in the rest frame of the medium by ω_m and \mathbf{k}_m , respectively. The dispersion relation in this frame, $|\mathbf{k}_m| = n\omega_m$, can be rewritten in a Lorentz invariant form as

$$k^2 - (n^2 - 1)\omega_m^2 = 0, \quad \omega_m = -\mathbf{k} \cdot \mathbf{u}_m, \quad (1)$$

where k^μ is the wave 4-vector and u_m^μ is the 4-velocity of the medium. The equation stays valid, with the replacement $\eta_{\mu\nu} \rightarrow g_{\mu\nu}$, for radiation propagating in an inhomogeneous medium around a gravitating body in a curved spacetime, provided the wavelength of the radiation

λ is much smaller than the typical scale l on which gravitational field and the properties of the medium are varying (*geometrical optics approximation*). In this limit, radiation propagates along *rays*, the paths in the spacetime given by the Hamiltonian of the form¹⁷

$$H = -\frac{1}{2}[k^2 - (n^2 - 1)\omega_m^2]. \quad (2)$$

The Hamiltonian is subject to the constraint $H = 0$. Rays can be viewed as worldlines of *light signals*, configurations of electromagnetic field localized in a volume extended over many λ 's, but still small in comparison with l .

The refractive index of a cold non-magnetic plasma can be expressed in terms of plasma frequency ω_{pl} , which in turn is given by electron number density N_e ,

$$n^2 = 1 - \frac{\omega_{\text{pl}}^2}{\omega_m^2}, \quad \omega_{\text{pl}}^2 = \frac{e^2}{\epsilon_0 m_e} N_e. \quad (3)$$

The resulting dispersion relation is

$$k^2 + \omega_{\text{pl}}^2 = 0. \quad (4)$$

The Hamiltonian, $H = -\frac{1}{2}(k^2 + \omega_{\text{pl}}^2)$, corresponds to a “particle” with variable mass $m \propto \omega_{\text{pl}}$. If we identify momentum p_μ canonically conjugated with spacetime coordinates x^μ with the covariant components of the wave 4-vector, $p_\mu = k_\mu$, the 4-velocity of the light signal will be $\dot{x}^\mu = k^\mu$, where the dot denotes differentiation with respect to the parameter of the ray. Note, however, that the *physical* momentum differs from k^μ ; in particular, for a single photon we have $p_{\text{phys}}^\mu = \hbar k^\mu$ and $m_{\text{phys}} = \hbar \omega_{\text{pl}}$.

Since the Hamiltonian for rays in cold plasma does not contain the frequency $\omega_m = -k \cdot u_m$, the propagation of light signals is not affected by the motion of plasma. Still, frequency ω_m enters the condition determining where the radiation can in principle be observed: the rays can penetrate only regions in which n is real, i.e., the inequality $\omega_m \geq \omega_{\text{pl}}$ is satisfied. We would need to add this condition to the theory if the form of the rays would be given just by Hamilton equations. However, the theory contains, apart from Hamilton equations, an additional constraint that the Hamiltonian, of which we know from the equations only that it is conserved, is to be zero. As a consequence, the light signals have $\omega_m = (\mathbf{k}_m^2 + \omega_{\text{pl}}^2)^{1/2}$, so the condition $\omega_m \geq \omega_{\text{pl}}$ is fulfilled automatically.

Consider Kerr metric in Boyer–Lindquist coordinates $(x^0, x^1, x^2, x^3) = (t, r, \theta, \phi)$ and suppose the space outside the horizon is filled with plasma with the same symmetries as are those of the metric. The system has mirror symmetry with respect to the equatorial plane ($\theta = \pi/2$), which makes it possible for rays to lie entirely in that plane. Metric tensor restricted to the equatorial plane is block diagonal,

$$g_{\mu\nu} = \begin{pmatrix} g^{AB} & 0 \\ 0 & g_{11} \end{pmatrix}, \text{ where } A, B = 0, 3, \text{ so } k^2 = g^{AB} k_A k_B + g_{11} \dot{r}^2 \text{ and we can rewrite the dispersion relation (4) as}$$

$$\dot{r}^2 = -g^{11}(g^{AB} k_A k_B + \omega_{\text{pl}}^2). \quad (5)$$

The covariant t - and ϕ -components of the wave 4-vector can be written as $k_0 = -\omega$ and $k_3 = \omega b$, where ω and b are frequency and impact parameter, respectively, measured by distant observers (assuming the rays can reach them). For the given values of ω and b , the signal can arrive at the given radius r only if the rhs of (5) is non-negative, the zero value corresponding either to a turning point or to a circular orbit.

Kerr metric depends on two parameters: the black hole mass M and the Kerr parameter a (angular momentum per unit mass). If we put $M = 1$, denote $u = r^{-1}$ and introduce functions $f = 1 - 2u$, $\mathcal{A} = 1 + a^2 u^2 + 2a^2 u^3$ and $\mathcal{D} = 1 - 2u + a^2 u^2$, the metric in the equatorial plane becomes

$$ds^2 = -f dt^2 - 4ar^{-1} dt d\phi + \mathcal{A} r^2 d\phi^2 + \mathcal{D}^{-1} dr^2.$$

Note that functions f , \mathcal{A} and \mathcal{D} satisfy the identity $f\mathcal{A} + 4a^2 u^4 = \mathcal{D}$. By inserting for g^{AB} , k_0 and k_3 , we obtain (denoting by superscript “ \circ ” the vacuum case)

$$g^{AB} k_A k_B = -\omega^2 \frac{\hat{F}}{\mathcal{D} r^2}, \quad \hat{F} = \mathcal{A} r^2 - 4ar^{-1} b - f b^2.$$

If we plug this into Eq. (5) and use $g^{11} = \mathcal{D}$, we find

$$\dot{r}^2 = \omega^2 F r^{-2}, \quad \text{where in plasma } F = \hat{F} - \mathcal{D} r^2 \frac{\omega_{\text{pl}}^2}{\omega^2}. \quad (6)$$

Light signals can propagate only in the regions in the (r, b) -plane with $F \geq 0$; they have turning points ($\dot{r} = 0$) at $F = 0$ and revolve around the black hole on a circular orbit if, in addition to $F = 0$, F also satisfies $F' = 0$ (prime denoting differentiation with respect to r).

We are interested in regions in the (r, b) -plane accessible to rays in the equatorial plane of Kerr black hole surrounded by plasma with the given electron number density N_e . We consider two situations: (i) the light signal propagating along the ray has a fixed frequency ω at infinity, or (ii) it has a fixed “telescope frequency” ω_0 seen by an observer with given 4-velocity u_{obs}^μ at the given radius r_0 . In the latter case the

spectrum of the light arriving at the observer, be it from distant sources (stars) or from a source close to the horizon, is supposed to spread across all frequencies ω , so that among the components of the light there is always one whose frequency in the observer's frame is ω_0 . For plasma, we will employ the model of a *nonsingular isothermal sphere* used, for example, in Refs. 28 and 30, in which $N_e \propto (r^2 + r_c^2)^{-1}$. In the problem with fixed "telescope frequency" we will consider first an observer at rest with respect to a given *locally nonrotating frame* (LNRF), and then an observer falling freely from rest at infinity.

The 4-velocity of a particle moving in the equatorial plane is $u^\mu = \Gamma(1, v, 0, \Omega)$, where v and Ω are radial and angular coordinate velocities, $v = dr/dt$ and $\Omega = d\phi/dt$; $\Gamma = dt/d\tau$ is the conversion factor between the time of distant observers t and the proper time τ of the particle. Let Ω and Γ be the angular velocity and the Lorentz factor of LNRF, $\Omega = 2au^3/\mathcal{A}$, $\Gamma = (\mathcal{A}/\mathcal{D})^{1/2}$, and \hat{v} and $\hat{\Gamma}$ be the (coordinate) radial velocity and the Lorentz factor of a particle falling freely from the rest at infinity, $\hat{v} = -\mathcal{D}\sqrt{\alpha}/\mathcal{A}$, where $\alpha = \mathcal{A} - \mathcal{D} = 2u(1 + a^2u^2)$, and $\hat{\Gamma} = \mathcal{A}/\mathcal{D}$. (This follows from separated geodesic equations – see Ref. 31 for a detailed discussion, including the integration in this case.) Using this notation, we have $v_{\text{obs}} = 0$, $\Omega_{\text{obs}} = \Omega_0$ and $\Gamma_{\text{obs}} = \Gamma_0$ (index 0 refers to the radius r_0) for a locally nonrotating observer, and $v_{\text{obs}} = \hat{v}_0$, $\Omega_{\text{obs}} = \Omega_0$, and $\Gamma_{\text{obs}} = \hat{\Gamma}_0$ for a freely falling observer.

The frequency seen by an observer with the 4-velocity u^μ_{obs} is $\omega_0 = -k \cdot u_{\text{obs}} = \omega\Gamma_{\text{obs}}(1 - \mathcal{D}_0^{-1}v_{\text{obs}}\eta_0 - \Omega_{\text{obs}}b)$, where η is the rescaled radial velocity of light, $\eta = \dot{r}_{\text{ph}}/\omega = \pm\sqrt{Fu}$ (index "ph" stands for "photon"). For the locally nonrotating observer this yields

$$\omega_0 = \omega\Gamma_0(1 - \Omega_0b), \tag{7}$$

and for the freely falling observer ($\xi = \mathcal{D}^{-1}\hat{v} = -\sqrt{\alpha}/\mathcal{A}$) we obtain

$$\omega_0 = \omega\hat{\Gamma}_0(1 - \xi_0\eta_0 - \Omega_0b). \tag{8}$$

III. RADIATION WITH FIXED ω

Consider first radiation in vacuum. The boundaries of allowed regions are given by the solutions to the quadratic equation $\dot{F} = 0$, which can be expressed in two equivalent forms,

$$\dot{b}_\pm = \frac{1}{f}(-2ar^{-1} \pm \sqrt{\mathcal{D}r}) = \frac{\mathcal{A}r^2}{2ar^{-1} \pm \sqrt{\mathcal{D}r}}. \tag{9}$$

Functions \dot{b}_\pm coincide at the horizon, $\dot{b}_\pm = b_h = \Omega_h^{-1}$ at $r = r_h = 1 + \sqrt{1 - a^2}$ (the larger root of $\mathcal{D} = 0$), and approach asymptotes at the angles $\pm 45^\circ$ to the r axis far from the horizon, $\dot{b}_\pm \sim \pm r$ for $r \gg 1$. From the first expression in (9) we can see that the \dot{b}_- root is falling to $-\infty$ and rising to $+\infty$ as we approach the radius $r = 2$ (static limit) from the left and right, respectively. From the second expression in (9), on the other hand, it is seen that the \dot{b}_+ root stays finite at $r = 2$. As seen in Fig. 1, there are two distinct regions in the (r, b) -diagram forbidden for the rays (regions where $\dot{F} < 0$): the "upper corner" above \dot{b}_+ at $r > 2$ and between \dot{b}_+ and \dot{b}_- at $r < 2$, and the "lower corner" under \dot{b}_- at $r > 2$. Outside the corners there are two regions accessible for rays, region \mathcal{O}_I between the corners at $r > 2$ and below the upper corner at $r < 2$, and region \mathcal{O}_{II} left to the upper corner at $r < 2$. Photon orbits are located at the lowest point of the upper corner (corotating orbit) and at the highest point of the lower corner (counter-rotating orbit).

Frequency of radiation seen by an observer with $v_{\text{obs}} = 0$ is $\omega_{\text{obs}} = \omega\Gamma_{\text{obs}}(1 - \Omega_{\text{obs}}b)$. This frequency is necessarily > 0 , hence we can determine the sign of ω at any given point in the (r, b) -plane by analyzing the interval of possible values of the angular velocity Ω_{obs} . Denote by Ω_\pm angular velocities of co- and counter-rotating light signals in vacuum, kept on a path close to a circle with an arbitrary given radius by a system of mirrors tangential to the circle and placed at equal distances from each other. The signals have, in the limit when the number of mirrors goes to infinity, $b = \dot{b}_\pm$, and their 4-velocity squared is $u_{\text{ph}}^2 = -\omega\dot{r}_{\text{ph}} + \kappa\dot{\phi}_{\text{ph}} \propto -1 + b\Omega_{\text{ph}} = 0$. Thus, \dot{b}_\pm are just inverses to Ω_\pm ; $\dot{b}_\pm = \Omega_\pm^{-1}$. The value of Ω_{obs} falls between Ω_{-0} and Ω_{+0} , therefore, $b/\dot{b}_{-0} < \Omega_{\text{obs}}b < b/\dot{b}_{+0}$ for $b > 0$ and $\Omega_{\text{obs}}b < b/\dot{b}_{-0}$ for $b < 0$. As a result, we have different signs of ω in different allowed regions: light signals have $\omega > 0$ in region \mathcal{O}_I and $\omega < 0$ in region \mathcal{O}_{II} . The radiation with $\omega < 0$ is a special case of a "particle" with a negative energy – a necessary ingredient of the Penrose process (see, e.g., Ref. 32, Sec. 33.7).

Now let us add plasma to the picture. Consider radiation with a fixed frequency ω at infinity, positive in region \mathcal{O}_I and negative in region \mathcal{O}_{II} . The function defining the boundaries of the allowed regions is now shifted, $F = \dot{F} - \mathcal{D}r^2\zeta^2$, where $\zeta = \omega_{\text{pl}}/\omega$. Equation $F = 0$ is again quadratic, and its solutions b_\pm can be written in the form of the first expression in (9) with $\mathcal{D} \rightarrow (1 - f\zeta^2)\mathcal{D}$ [Eq. (A1)]. We can see that functions b_\pm have the same asymptotes at $r \gg 1$ as functions \dot{b}_\pm , $b_\pm \sim \pm r$, and that the asymptote of function b_- , with b_- falling to $-\infty$ to the right of it and rising to $+\infty$ to the left of it, lies at $r = 2$ just like that of function \dot{b}_- . However, the similarity between functions \dot{b}_- and b_\pm ends there: b_\pm , when compared to \dot{b}_\pm , are pulled towards each other or entirely vanish at $r > 2$, and are pushed away from each other at $r < 2$. As a result, both forbidden regions expand, and there may even appear a neck between them, so that no ray, regardless of its impact parameter, can pass from black hole to distant observers or vice versa. The formation of the neck is discussed in Appendix A.

As the forbidden regions expand, allowed regions shrink: instead of regions \mathcal{O}_I and \mathcal{O}_{II} in vacuum we have smaller regions \mathcal{O}_I and \mathcal{O}_{II} contained within them. The former region is divided into two parts in the presence of a neck, \mathcal{O}_{IA} on the lower left of the neck and \mathcal{O}_{IB} on its right. Since \mathcal{O}_I and \mathcal{O}_{II} lie inside \mathcal{O}_I and \mathcal{O}_{II} , we have $\omega > 0$ in the former region and $\omega < 0$ in the latter one.

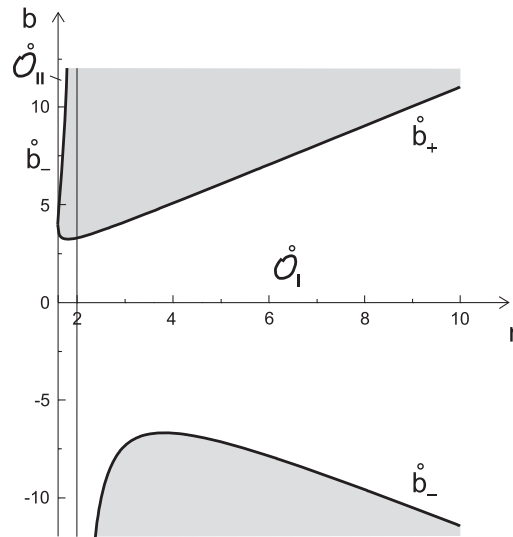


FIG. 1. Allowed regions for rays in vacuum. Kerr parameter is $a = 0.8$ and radius of the horizon is $r_h = 1.6$. Shaded areas bounded by the lines b_+ and b_- (“corners”) are forbidden, free areas \mathcal{O}_I and \mathcal{O}_{II} outside them are allowed. The thin vertical line at $r = 2$ is the asymptote of the inner boundary of forbidden regions.

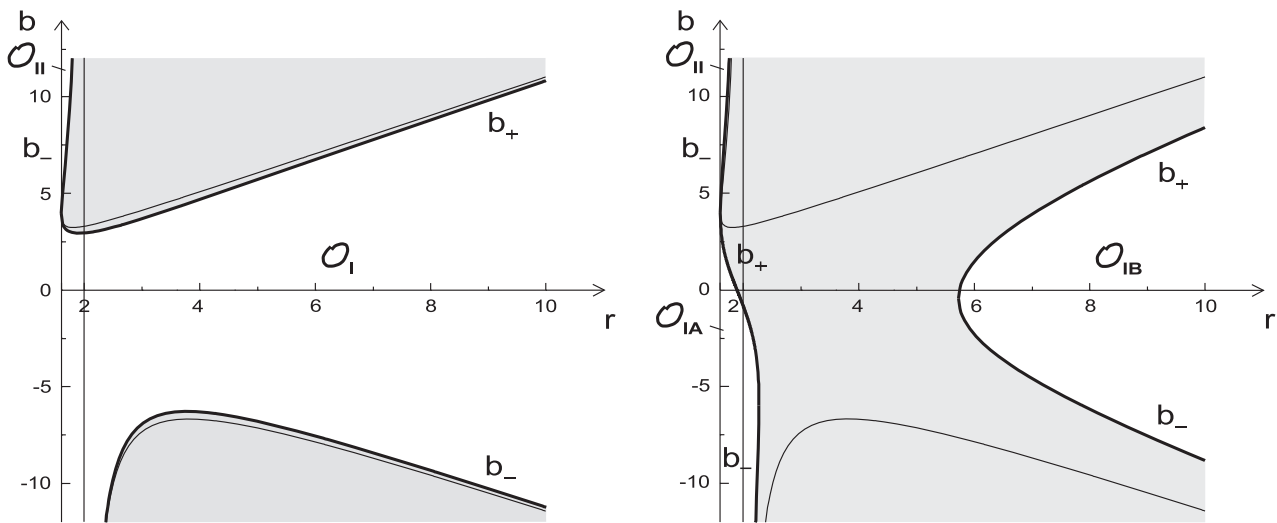


FIG. 2. Allowed regions for rays in plasma with fixed frequency ω at infinity. In addition to $a = 0.8$ we have $r_c = 1$, $r_{ref} = 1.8$ (the reference circle lies halfway between the horizon and the static limit) and $q = 1, 3.5$ in the left and right panel, respectively. Shaded areas are forbidden, free areas outside them, regions \mathcal{O}_I and \mathcal{O}_{II} in the left panel and regions \mathcal{O}_{IA} , \mathcal{O}_{IB} and \mathcal{O}_{II} in the right panel, are allowed. For comparison, the boundaries of forbidden regions in vacuum are shown, too, depicted by lighter lines inside the shaded regions. The vertical line, located at the static limit just like in vacuum, is the asymptote of the inner boundary of the forbidden regions, separated from each other in the left panel and connected by a neck in the right panel. Radiation has $\omega > 0$ in region \mathcal{O}_I , divided into regions \mathcal{O}_{IA} and \mathcal{O}_{IB} in the right panel, and $\omega < 0$ in region \mathcal{O}_{II} .

Function ζ is proportional to ω_{pl} , hence to $\sqrt{N_e}$, so, for our choice of plasma distribution, to $(r^2 + r_c^2)^{-1/2}$. To fix the coefficient of proportionality, we choose some radius r_{ref} close to r_h and some frequency ratio $q = \omega_{pl,ref}/|\omega|$, and write $\zeta = \pm q\sqrt{\mathcal{R}}$, where $\mathcal{R} = N_e/N_{e,ref} = (r_{ref}^2 + r_c^2)/(r^2 + r_c^2)$; the signs $+$ and $-$ refer to region \mathcal{O}_I and \mathcal{O}_{II} , respectively.

Allowed regions for radiation with fixed ω are shown in Fig. 2. As expected, forbidden regions in plasma are larger as compared with those in vacuum. In the right panel q exceeds q_{crit} defined in Appendix A, therefore forbidden regions are connected by a neck.

IV. RADIATION WITH FIXED ω_0 : LNRFB OBSERVERS

Consider a LNRFB observer at $r = r_0$, with the telescope adjusted to frequency ω_0 . Then, we can use Eq. (7) to express $\zeta = \omega_{pl}/\omega$ in terms of ω_0 . In this way we obtain

$$\zeta = \pm q \Gamma_0 (1 - \Omega_0 b) \sqrt{\mathcal{R}}, \quad (10)$$

where q is the ratio of the plasma frequency on observer's orbit to the absolute value of the telescope frequency, $q = \omega_{pl,0}/|\omega_0|$, \mathcal{R} is the electron density ratio for $r_{ref} = r_0$, $\mathcal{R} = N_e/N_{e0} = (r_0^2 + r_c^2)/(r^2 + r_c^2)$, and the sign in front of q equals the relative sign of ω and ω_0 . (For the possibility of $\omega_0 < 0$, see below.) In what follows we assume that q is independent of r_0 so that observers set on different orbits have different telescope frequencies, the less the larger the radius of the orbit; in such a way they are able to see the effect of plasma on the propagation of radiation even at $r \gg 1$, where plasma is thin. If *plasma* is locally nonrotating, we have $\omega_{m0} = \omega_0$ and the condition of real-valuedness of n implies that no ray can reach the observer unless $q < 1$. However, since n is real in the regions where $F \geq 0$ regardless of how the plasma moves, the constraint on q has to be satisfied in general case as well [as seen also from Eq. (D1), where there appears $1 - q^2$ under the square root].

If we insert into $F = \dot{F} - \mathcal{D}r^2 \zeta^2$ from (10), we see that F is quadratic in b just as in the case with fixed ω , when $\zeta = const$; however, all three coefficients in expression $F = k + 2lb + mb^2$ now become shifted, not just k [Eq. (B1)]. This manifests itself in the behavior of functions b_{\pm} solving equation $F = 0$. In particular, the shift in m implies that the asymptotics of b_{\pm} at $r \gg 1$ is modified to $b_{\pm} \sim \pm Cr$, where $C < 1$, and that the radius r_a of the asymptote of function b_{-} shifts from $r_a = 2$ to $r_a < 2$. In Appendix B we show that C increases from 0 to 1 and r_a increases from r_h to 2, as the radius of observer's orbit r_0 increases from r_h to ∞ . We also discuss there the case when the function diverging at r_a is b_{+} rather than b_{-} .

Forbidden regions in the (r, b) -plane may be connected by a neck just as in the case with fixed ω . The neck is formed in an interval of r where $\Delta = l^2 - km < 0$ (the discriminant of equation $F = 0$ is negative). As shown in Appendix C, the neck is there for $r_0 \sim r_h$ as well as for $r_0 \gg 1$, but it disappears in some interval $\rho_{0A} < r_0 < \rho_{0B}$. The band connecting forbidden regions shrinks to a point at some radius $r = \rho_A$, as r_0 approaches the value ρ_{0A} from the left, and at some radius $r = \rho_B > \rho_A$, as r_0 approaches the value ρ_{0B} from the right. The values of the radii (ρ_{0A}, ρ_A) and (ρ_{0B}, ρ_B) are discussed in Appendix C.

With ω_0 fixed, we can either restrict to the rays that actually reach the observer, or to consider also "ghost rays" that bounce on their way back to the observer, but have such frequency ω and impact parameter b that their frequency measured by the observer, provided they reach them, would have just the desired value. In the latter case we obtain allowed regions \mathcal{O}_I and \mathcal{O}_{II} similar in form to those in the problem with fixed ω . The frequency ω_0 , however, must be taken with minus sign for some "ghost rays," depending on the value of b when compared to the limit impact parameter $b_{lim} = \Omega_0^{-1}$. By (7), $\omega_0 \propto \omega(1 - b/b_{lim})$, and since $\omega > 0$ in \mathcal{O}_I and $\omega < 0$ in \mathcal{O}_{II} , we need to put $\omega_0 < 0$ in the upper part of \mathcal{O}_I , where $b > b_{lim}$, as well as in the lower part of \mathcal{O}_{II} , where $b < b_{lim}$.

Allowed regions for radiation with fixed ω_0 are shown in Fig. 2. The areas bounded by thick lines are allowed regions for rays that eventually reach the observer, either directly or after bouncing back. The remaining free areas outside the shaded corners, or shaded strip in the case with a neck, are allowed regions for "ghost rays" that never arrive at the observer.

In the left panel, r_0 is in the interval (ρ_{0A}, ρ_{0B}) , therefore the corners are separated from each other and rays can propagate freely from infinity to the horizon and back within free band \mathcal{F} . Outside \mathcal{F} there are allowed regions bounded from one side: if r_0 is less than the radius at which b_{+} has minimum, as in the figure, rays can reach the observer from the regions \mathcal{G}_{I+} , \mathcal{G}_{I-} adjacent to \mathcal{F} and (not seen in the figure) region \mathcal{G}_{II} separated from \mathcal{F} , all bounded from outside. In the right panel, r_0 lies outside the interval (ρ_{0A}, ρ_{0B}) , hence the corners merge and rays accessible to the observer are restricted to regions \mathcal{G}_{IA} and \mathcal{G}_{II} bounded from outside for $r_0 < \rho_{0A}$ (left part of the panel) and region \mathcal{G}_{IB} bounded from inside for $r_0 > \rho_{0B}$ (right part of the panel). In the case with $r_0 < \rho_{0A}$, we have $q < q_{rev}$, with q_{rev} defined in Appendix B; hence, the asymptote at $r = r_a$ is approached by function b_{-} .

Rays accessible to the LNRFB observers, who are orbiting the black hole at different radii r_0 , occupy regions $\tilde{\mathcal{O}}_I$ and $\tilde{\mathcal{O}}_{II}$ in the (r_0, b) -plane, similar in form to regions \mathcal{O}_I and \mathcal{O}_{II} in the problem with fixed ω and $q < q_{crit}$ (left panel of Fig. 2), with the boundaries B_{\pm} given by equation $F(r = r_0) = 0$. As shown in Appendix D, functions B_{\pm} are given by the second expression in (9), with r replaced by r_0 and with the function under the square root rescaled as $\mathcal{D}_0 \rightarrow \mathcal{D}_0/(1 - q^2)$ [Eq. (D1)].

In the allowed regions in (r_0, b) -plane there are *two* rays with the telescope frequency passing through each point, one directed towards the black hole (with $\dot{r}_{ph,0} < 0$) and one directed away from it (with $\dot{r}_{ph,0} > 0$). Let us single out two distinct parts of the allowed regions by the behavior of rays extended backwards in time, region \mathcal{O}_h in which at least one of the rays starts at the horizon and region \mathcal{O}_i in which at least one of the rays starts at infinity (in the sense of limit) – see Fig. 4. Denote, furthermore, by \mathcal{O}_{h+i} the intersection of \mathcal{O}_h and \mathcal{O}_i and by \mathcal{O}'_h and \mathcal{O}'_i the parts of \mathcal{O}_h and \mathcal{O}_i outside of \mathcal{O}_{h+i} . Region \mathcal{O}_{h+i} consists of rays from the free bands in the (r, b) -plane, like band \mathcal{F} in the left panel of Fig. 3, while regions \mathcal{O}'_h and \mathcal{O}'_i are composed of rays from allowed regions bounded from one side, like regions \mathcal{G}_{I+} and \mathcal{G}_{I-} in the left panel of Fig. 3 and regions \mathcal{G}_{IA} , \mathcal{G}_{II} and \mathcal{G}_{IB} in the right panel of Fig. 3. If we denote by B_{+} the upper limit of \mathcal{F} (minimum of b_{+}) and by B_{-} the lower limit of \mathcal{F} (maximum of b_{-} for $r > r_a$), we can define \mathcal{O}_{h+i} as a region in the (r_0, b) -plane bounded from above by the line B_{+} and from below by the line B_{-} . Note that the boundaries actually do not belong to \mathcal{O}_{h+i} , since for rays with $b = B_{\pm}$ the access to the observer is free from one side only; when arriving from the other side, the rays do not get past the peak of the forbidden corner standing in their way. Since the radii R_{\pm} , where b_{+} has minimum and b_{-} has maximum, depend continuously on the radius r_0 , and since $R_{\pm} > r_0$ at $r_0 = \rho_{0A}$ and $R_{\pm} < r_0$ at $r_0 = \rho_{0B}$, r_0 eventually passes through R_{+} as well as R_{-} as it rises from ρ_{0A} to ρ_{0B} . As a result, lines B_{\pm} touch lines B_{\pm} in some points P_{\pm} , dividing the boundary of region \mathcal{O}_{h+i} into two segments where regions \mathcal{O}'_h and \mathcal{O}'_i are attached to region \mathcal{O}_{h+i} , \mathcal{O}'_h from the left and \mathcal{O}'_i from the right. The position of points P_{\pm} as well as the behavior of functions B_{\pm} , \mathcal{B}_{\pm} in their vicinity are discussed in Appendix D.

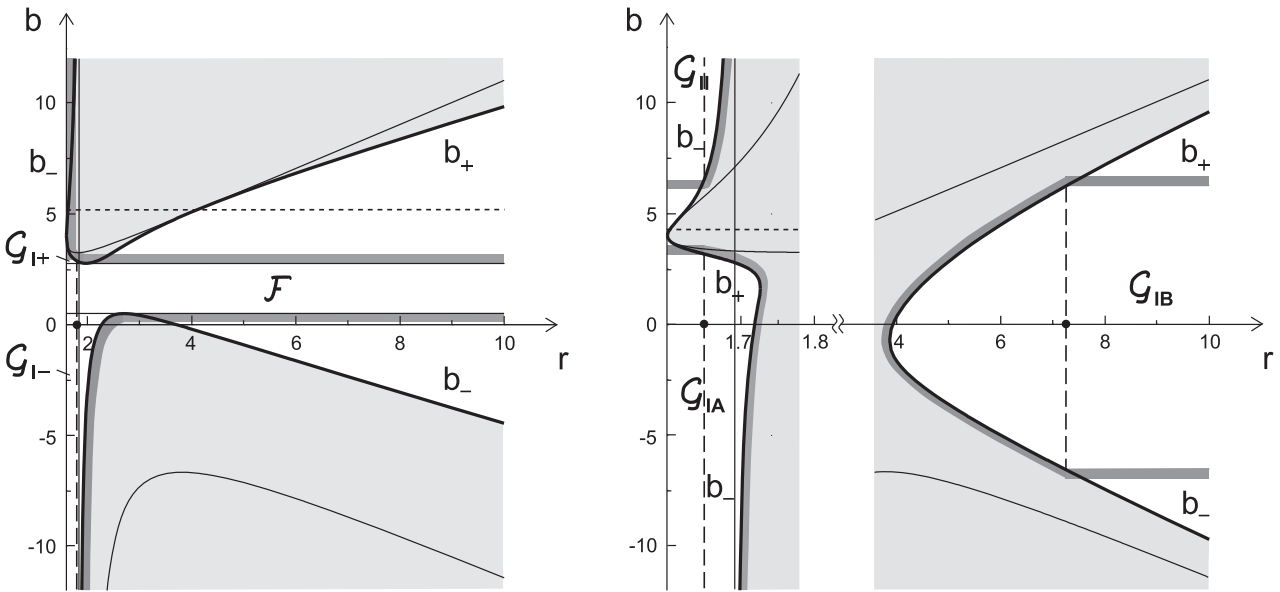


FIG. 3. Allowed regions for rays in plasma with fixed frequency ω_0 seen by a LNRF observer. In addition to $a = 0.8$ and $r_c = 1$ we have $q = 2/3$ and $r_0 = 1.8, 1.65$ and 7.25 in the left panel, left part of the right panel and right part of the right panel, respectively. Shaded areas are forbidden regions in an extended theory with “ghost rays,” thin lines inside them indicate where the forbidden regions lie in vacuum, solid vertical line is the asymptote of the inner boundary of forbidden regions and dotted horizontal line represents b_{lim} , the value of b dividing regions with “ghost rays” in the upper part of the diagrams into two parts with different sign of ω_0 : in order that ω has the right sign, ω_0 needs to be <0 above b_{lim} for $r > 2$ and under b_{lim} for $r < 2$ and $b > b_h$. Position of the observer is marked by a bullet on the r axis, dashed lines depict rays at the moment of arriving at the observer and areas within the thick lines, regions \mathcal{F} , \mathcal{G}_{I+} and \mathcal{G}_{I-} in the left panel and \mathcal{G}_{IA} , \mathcal{G}_{II} and \mathcal{G}_{IB} in the right panel, are allowed regions for rays reaching the observer. Region \mathcal{G}_{II} in the left panel and line b_{lim} in the right part of the right panel did not make it into the diagram since they lie too high, the former at $b > 25.7$ and the latter at $b = 276.5$.

Allowed regions for rays seen by LNRF observers at various distances from the black hole are shown in Fig. 4.

Region \mathcal{O}_h , consisting of \mathcal{O}_{h+i} in the center of $\tilde{\mathcal{O}}_I$, region \mathcal{O}'_{h-} adjacent to it and region $\mathcal{O}'_{h+} = \tilde{\mathcal{O}}_{II}$ disconnected from both of them, is shown in the left panel. Region \mathcal{O}_i , composed of regions \mathcal{O}_{h+i} and \mathcal{O}'_i , is displayed in the right panel. The Kerr parameter is less than critical, $a < a_{crit}$, where a_{crit} is defined in Appendix D, therefore the point P_+ is shifted to the left of the static limit. The boundary of region \mathcal{O}_{h+i} is not horizontal at points P_{\pm} as it may appear from the figure; instead, as discussed in Appendix D, it is slightly inclined downwards at P_+ and upwards at P_- .

V. RADIATION WITH FIXED ω_0 : FREELY FALLING OBSERVERS

As seen from Eq. (8), the ratio $\zeta = \omega_{pl}/\omega$ for an observer falling freely from rest at infinity can be written as

$$\zeta = q\hat{\Gamma}_0(1 - \xi_0\eta_0 - \Omega_0 b)\sqrt{\mathcal{R}}. \quad (11)$$

The expression is applicable only to rays that can reach the observer, otherwise the parameter $\eta_0 = \pm\sqrt{F_0}u_0$ is purely imaginary. Thus, the frequency ω_0 is necessarily positive; unlike in the case of locally nonrotating observer, there exist no, “ghost rays” with $\omega_0 = -|\omega_0|$. As a result, parameter q can be defined just as $q = \omega_{pl,0}/\omega_0$ and no \pm is needed in Eq. (11).

Function $\mathcal{F} = Fu^2$ satisfies the identity $\mathcal{F}_0 = \eta_0^2$, which can be written as a quadratic equation for η_0 : $K_0 + 2L_0\eta_0 + M_0\eta_0^2 = 0$. We can define allowed regions $\tilde{\mathcal{O}}_I$ and $\tilde{\mathcal{O}}_{II}$ in the (r_0, b) -plane by the condition $\mathcal{F}_0 \geq 0$ just as for the LNRF observers, however, now this inequality is not saturated at the boundaries of $\tilde{\mathcal{O}}_I$ and $\tilde{\mathcal{O}}_{II}$. Therefore, if we want to determine the shape of these regions, we need to start from the requirement that equation $\mathcal{F}_0 = \eta_0^2$ has real solution, i.e., from the inequality $\delta_0 = L_0^2 - K_0M_0 \geq 0$. As shown in Appendix E, this leads to the boundaries \tilde{B}_{\pm} which are given by the same expression as the boundaries B_{\pm} in the problem with LNRF observers, just with q replaced by $\tilde{q}_{NR} = q\hat{\Gamma}_0/[1 + q^2(\hat{\Gamma}_0^2 - 1)]^{1/2}$. If we choose q as a function of r_0 so that $\tilde{q}_{NR} = const$, regions $\tilde{\mathcal{O}}_I$ and $\tilde{\mathcal{O}}_{II}$ will have the same shape for freely falling observers as for locally nonrotating ones.

We have again, as in the problem with LNRF observers, two rays at each point of regions $\tilde{\mathcal{O}}_I$ and $\tilde{\mathcal{O}}_{II}$; however, the rays now have rescaled radial velocities $\eta_0^{(\pm)} = (-L_0 \pm \sqrt{\delta_0})/M_0$ which do not differ just by sign. They can even have the same sign: $\eta_0^{(-)}$ is negative in the whole region $\tilde{\mathcal{O}}_I$, including its boundaries, but $\eta_0^{(+)}$ is positive in a smaller region, passing through zero at lines B_{\pm} where $K_0 = 0$. In region $\tilde{\mathcal{O}}_{II}$, on the other hand, $\eta_0^{(+)}$ is positive everywhere and $\eta_0^{(-)}$ is negative outside the line B_- . However, $\dot{r}_{ph,0}$ has sign different from η_0 in region $\tilde{\mathcal{O}}_{II}$,

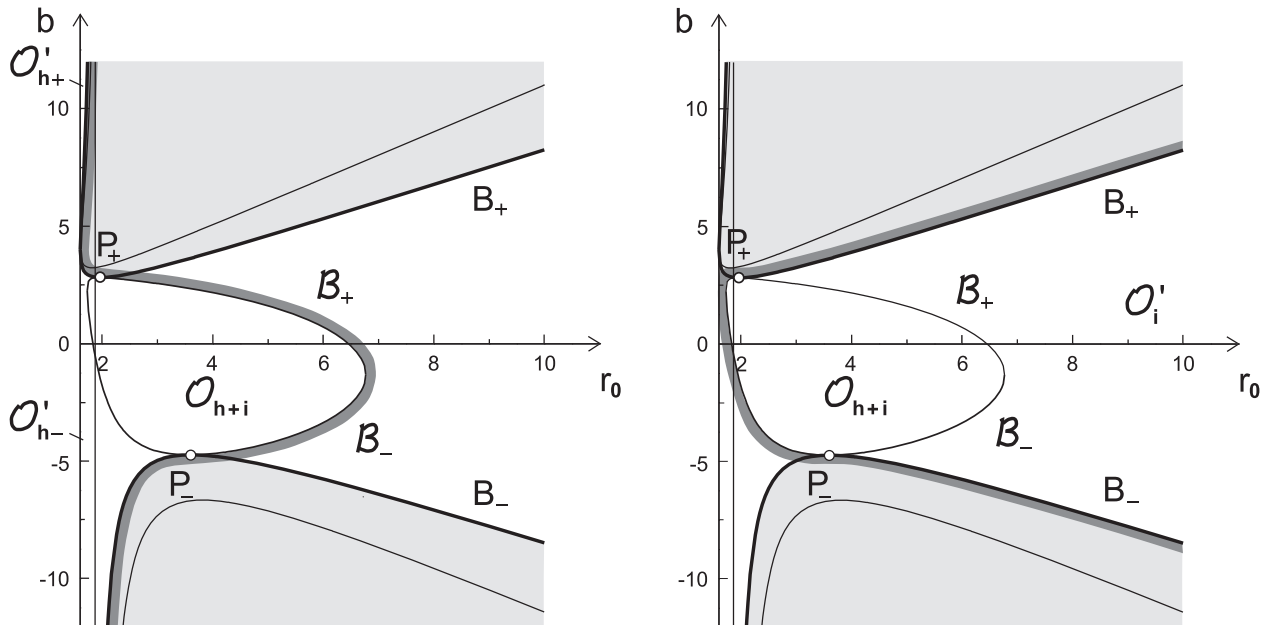


FIG. 4. Allowed regions in the (r_0, b) plane for radiation seen by LNRF observers. Parameters a , r_c and q are the same as in Fig. 3. Shaded areas are forbidden for rays seen by the observer at the given radius r_0 , thin lines inside them are boundaries of the forbidden regions in vacuum [they look the same in the (r_0, b) plane as in the (r, b) plane, since the form of rays in vacuum does not depend on ω], solid vertical line is the asymptote of the inner boundary of forbidden regions, region \mathcal{O}_{h+i} in the central part of the diagrams consists of rays that can reach observers from the horizon as well as from infinity, regions $\mathcal{O}'_{h\pm}$ in the left panel and region \mathcal{O}'_i in the right panel are composed of rays that can reach observers from one side only, either from the horizon (regions $\mathcal{O}'_{h\pm}$) or and from infinity (region \mathcal{O}'_i), and points P_{\pm} divide the boundary of \mathcal{O}_{h+i} into segments adjacent to these regions. Rays that can come to the local observers from the horizon form the region \mathcal{O}_h to the left of the thick line in the left panel, and rays that can arrive at the local observers from infinity comprise the region \mathcal{O}_i to the right of the thick line in the right panel.

since it equals $\omega\eta_0$ and $\omega < 0$ there. Let us call rays with velocities $\eta_0^{(+)}$ in region $\tilde{\mathcal{O}}_I$ and $\eta_0^{(-)}$ in region $\tilde{\mathcal{O}}_{II}$ “rays of class I,” and rays with the other velocities “rays of class II.” As suggested by the discussion of the signs of $\eta_0^{(\pm)}$, the rays of class II, as well as the rays of class I, lying between the lines \tilde{B}_{\pm} and B_{\pm} , are directed towards the horizon, while the remaining rays of class I are directed away from it.

Should we define regions \mathcal{O}_h and \mathcal{O}_i as before, we would have diagrams containing the rays of both classes I and II, with region \mathcal{O}_{h+i} divided into three zones, each with rays of different behavior.

We will consider the two classes separately, extending the definition of regions \mathcal{O}_h and \mathcal{O}_i by using rays prolonged in both directions in time: the ray will be supposed to belong to region \mathcal{O}_h if it has, when maximally extended, either starting or ending point on the horizon, and to region \mathcal{O}_i , respectively, if it has either starting or ending point at infinity.

Allowed regions for rays seen by freely falling observers at various distances from black hole are depicted in Fig. 5. In the left panel we show the behavior of rays of class I, in the right panel – of class II. Regions \mathcal{O}_h and \mathcal{O}_i are displayed both in the same diagram, marked by continuous and intermittent thick line, respectively. In Appendix E we explain how we determined those regions without having an explicit expression for the boundaries of forbidden regions in the (r, b) -plane. If we return to the original definition of regions \mathcal{O}_h and \mathcal{O}_i , the whole region \mathcal{O}_{h+i} in the right panel, as well as the part of region \mathcal{O}_{h+i} lying between the lines \tilde{B}_{\pm} and B_{\pm} in the left panel, will pass to region \mathcal{O}'_i , while the rest of region \mathcal{O}_{h+i} in the left panel will become a part of region \mathcal{O}'_h .

Since the rays with limit impact parameters \tilde{B}_{\pm} have nonzero rescaled radial velocities $\tilde{\eta}_0 = -L_0/M_0$, they do not bounce back as they arrive at the observer; instead, rays coming from infinity bounce back after they pass by the observer and rays coming from the horizon bounce back before that (as both have radial velocity $\tilde{r}_{ph,0} = \omega\tilde{\eta}_0 < 0$). In addition, there are also rays which, rather than bouncing back, proceed directly from infinity to the horizon. These rays form arcs $P_{A+}P_{B+}$ and $P_{A-}P_{B-}$, marked by the black segments of thick lines in Fig. 5. Similarly as the points P_+ and P_- in case of LNRF observers, arcs $P_{A+}P_{B+}$ and $P_{A-}P_{B-}$ divide the boundary of region \mathcal{O}_{h+i} into segments where it borders on regions \mathcal{O}'_h and \mathcal{O}'_i .

For rays of class I, allowed region $\tilde{\mathcal{O}}_I$ between line \tilde{B}_+ and the lower line \tilde{B}_- contains a smaller region $\tilde{\mathcal{O}}'_I$ between line B_+ and the lower line B_- , where rays do bounce back when arriving at the observer. (As explained in Appendix E, in order that the latter region extends to the horizon as in Fig. 5, \tilde{q}_{NR} needs to be $< 1/\sqrt{2}$.) At lines B_{\pm} , region \mathcal{O}_{h+i} shrinks to a point. Thus, it is composed of two triangles and a central part, attached to the boundaries of region \mathcal{O}'_i at some points Q_{\pm} , just as in the problem with LNRF observers region \mathcal{O}_{h+i} touched the boundaries of region $\tilde{\mathcal{O}}_I$ at points P_{\pm} . For rays of class II, region \mathcal{O}_{h+i} is considerably wider than for rays of class I; it also does not stop at a

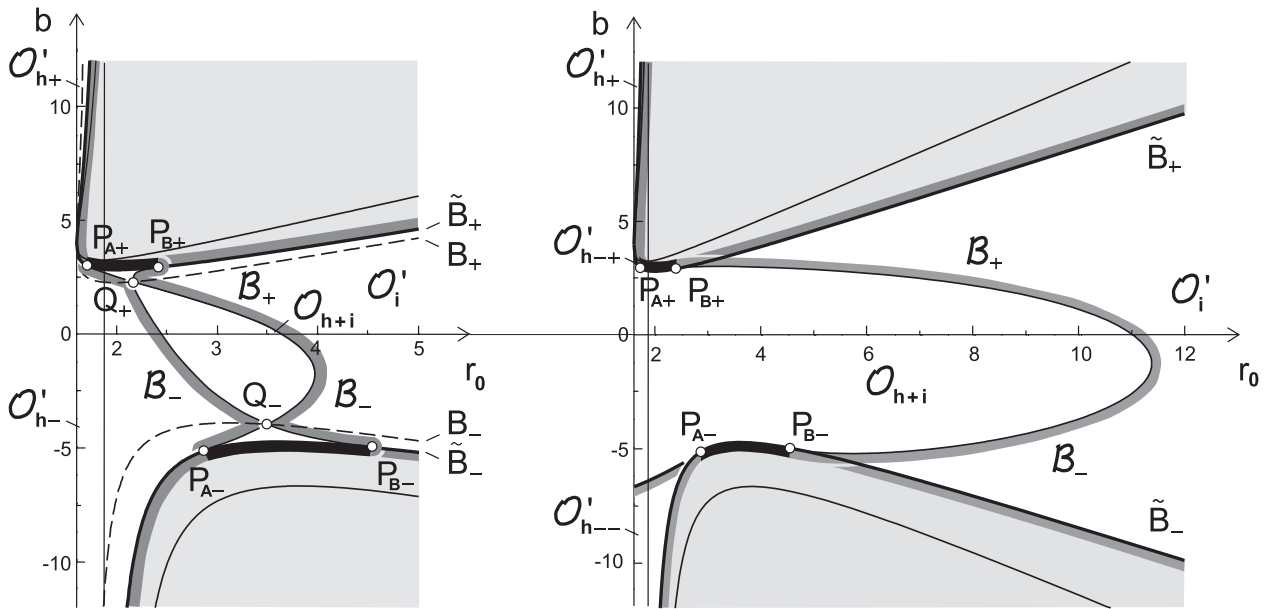


FIG. 5. Allowed regions in the (r_0, b) plane for radiation seen by freely falling observers from rest at infinity. Parameter a is the same as in Figs. 1–4, parameter r_c is the same as in Figs. 2–4 and parameter \tilde{q}_{NR} coincides with q used in Fig. 4. Allowed regions for rays of class I (with radial velocity $r_0^{(+)}$) and of class II (with radial velocity $r_0^{(-)}$) are shown in the left and right panel, respectively. The meaning of shaded areas, thin lines inside them and solid vertical line is the same as in Fig. 4, a new feature are only lines B_{\pm} (dashed lines in the left panel), where velocity $r_0^{(+)}$ changes its sign. Thick lines mark, as in Fig. 4, regions \mathcal{O}_h and \mathcal{O}_i ; both are now drawn in the same diagram, boundary of \mathcal{O}_h as continuous (“put on the top”) and boundary of \mathcal{O}_i as intermittent (“lying under it”). For rays of class I, region \mathcal{O}_h contains, in addition to region \mathcal{O}_{h+i} , regions $\mathcal{O}'_{h\pm}$ to the left of \mathcal{O}_{h+i} , and region \mathcal{O}_i contains region \mathcal{O}'_i to the right of \mathcal{O}_{h+i} , just as in Fig. 4; for rays of class II, region \mathcal{O}_{h+i} extends all the way down to the horizon and region \mathcal{O}'_{h-} is divided into regions \mathcal{O}'_{h-+} and \mathcal{O}'_{h--} , adjacent to \mathcal{O}_{h+i} from above and from below, respectively. Points P_{\pm} , where region \mathcal{O}_{h+i} has touched forbidden regions in the problem with LNRF observers, are stretched into finite segments, the same for rays of both classes (arcs $P_{A+}P_{B+}$ and $P_{A-}P_{B-}$ marked by thick black line). For rays of class I, broken arcs $P_{A+}P_{A-}$ and $P_{B+}P_{B-}$, forming together the boundary of \mathcal{O}_{h+i} , merge at the points Q_{\pm} lying on the lines B_{\pm} .

finite distance from the horizon, but extends all the way down. The shape of allowed regions for rays of both classes I and II is discussed in more detail in Appendix E.

VI. CONCLUSIONS

Using the Hamiltonian approach for tracing rays in curved spacetime possibly filled with dispersive and refractive medium, we studied their behavior in the Kerr metric. We restricted to equatorial plane and focused on comparing the form of the regions accessible to rays in vacuum case with the case when the black hole is surrounded by cold plasma. We assumed that plasma has distribution of an isothermal nonsingular sphere with inhomogeneity parameter comparable with the size of the black hole and with the density large enough to affect the propagation of radiation substantially.

In the presence of plasma, forbidden regions in the radius–impact parameter plane, the (r, b) -plane, become larger than in vacuum. They can even develop a neck preventing rays from passing from infinity to the horizon and back. To understand these effects, note that the plasma is acting on a ray *repulsively* if its density decreases with radius. Thus, rays are less bent in plasma than in vacuum, and since extremal values of b at given r correspond to rays tangent to the circle with radius r , plasma necessarily makes these values less in absolute value in case the rays are coming from infinity. (If such a ray is straightened, it needs to enter gravitational field closer to the radial line parallel to it, in order to get to the same distance from the source.) The neck connecting forbidden regions is formed when the repulsive effect is large enough to cause signals coming from infinity to bounce back, even if they have impact parameter b close to zero. As for signals coming from the horizon, it might seem that since they are dragged away from the black hole by plasma, no matter how small the repulsive effect is near the horizon, they necessarily escape from the black hole. However, in the expression for radial acceleration of a light signal there appears, in addition to a centrifugal acceleration proportional to b^2 , the term (with plus sign) proportional to r^2 . Since that term is less in the presence of plasma than in vacuum, the effect of gravity is enhanced by the presence of plasma, and if the plasma is dense enough, signals coming from the horizon bounce back.

We considered also observers located at various radii r_0 , equipped with telescopes with a given frequency ω_0 , and constructed allowed regions for rays with that frequency. LNRF observers were supposed to have frequency ω_0 proportional to the local plasma frequency, while for freely falling observers we added an extra factor rising to infinity as the observer’s Lorentzian factor Γ_0 , as the horizon is approached. Frequency of light signals with the extremal values of b blue-shifts by a factor of order Γ_0 as we pass from the LNRF to the freely falling frame,

hence it needs to be finite in the LNRF, just like the telescope frequency with LNRF observers. The frequency is blue-shifted despite the fact that the observer is moving away from the source, because of the transversal Doppler effect. However, rays coming from infinity can reach the horizon only if their impact parameter is separated by a finite gap from the maximum b in the region with positive frequency at infinity ω ; and with such b , rays with the velocity directed to the black hole are redshifted rather than blueshifted by the transition from the LNRF to the observer's frame. Their redshift is quite substantial, of order Γ_0^{-1} , so that their frequency in the LNRF is of the same order of magnitude as the Lorentzian factor $\tilde{\Gamma}_0 = \Gamma_0^2$ of a freely falling observer.

In the diagrams with multiple observers we constructed regions in which at least one of the two rays passing through each point of the diagram started at the horizon (region \mathcal{O}_h) or at infinity (region \mathcal{O}_i). The setting with freely falling observers is more general than that with LNRF observers, since the rays seen by them are independent of each other. For LNRF observers, the rays are related by a simultaneous change of sign of coordinates t and ϕ ; thus, they are mirror images of each other with respect to the radial line drawn through the point of observation, while their velocities are mirror images of each other with respect to the *tangential* line drawn through that point. As a result, the starting point of each ray, obtained by extending it maximally backwards in time, coincides with the ending point of the other ray, obtained by extending it maximally *forwards* in time, provided it passed by the observer without being detected. For freely falling observers the two rays are not mirror images of each other, since the radial motion of the observer breaks the symmetry with respect to the tangential line. Thus, we have two classes of rays that are *not* related by symmetry, one containing a subclass of rays directed away from the black hole and the other consisting entirely of rays directed towards the black hole. By extending the rays in both directions in time we obtain a separate diagram for each class. The diagrams look quite different from the one constructed with LNRF observers: the intersection of regions \mathcal{O}_h and \mathcal{O}_i is a narrow strip with ragged boundary, located close to the horizon, for rays of the first class, and a wide band with smooth boundary, reaching far from the horizon on one side and adjacent to the horizon on the other side, for rays of the second class.

Regions \mathcal{O}_h and \mathcal{O}_i arise in the diagrams with multiple observers because of the presence of plasma; they reflect the fact that if the plasma is sufficiently dense, there may appear necks in the diagrams with one observer. No such regions exist for rays in vacuum, whose form does not depend on frequency. Thus, the shape of regions \mathcal{O}_h and \mathcal{O}_i may be regarded as a visualization of the interplay between strong gravitational field and plasma as an example of a refractive and dispersive medium, as they act on radiation propagating through them.

The analysis can be extended outside the equatorial plane if the plasma has electron density depending on the coordinates r and θ in such a way that we have, in addition to the constants of motion ω and b , also the constant of motion K (Carter constant), just like in vacuum. In Ref. 14 the shape of the shadow of a black hole is calculated for three plasma distributions of the desired form, and for an observer who sees the photons of principal null congruences moving radially towards the black hole or away from it. The shadow is determined for radiation with fixed frequency at infinity ω , but the calculation can be easily modified to the case with fixed telescope frequency ω_0 , we just need to multiply the terms coming from ω_{pl}^2 in the equations for spherical rays by Q^2 , where Q is defined in terms of observer's angular velocity $\tilde{\Omega}_0$ and Lorentz factor $\tilde{\Gamma}_0$ as $Q = \tilde{\Gamma}_0(1 - \tilde{\Omega}_0 b)$. We have found that the region around the black hole where there exist spherical rays (photon region) as well as the black hole shadow shrink substantially as we pass from radiation with fixed ω to radiation with fixed ω_0 .

ACKNOWLEDGMENTS

V.B. was supported by the Grant No. VEGA 1/0719/23, B.B. acknowledges the support of the Charles University Grant Agency under the Contract No. 317421 and of the Charles University Grant No. UNCE24/SCI/016, B.B. and J.B. were supported by the Czech Grant Agency under the Contract No. 21/112685.

AUTHOR DECLARATIONS

Conflict of Interest

The authors have no conflicts to disclose.

Author Contributions

Vladimír Balek: Formal analysis (equal); Methodology (lead); Writing – original draft (lead). **Barbora Bezděková**: Formal analysis (equal); Writing – review & editing (supporting). **Jiří Bičák**: Conceptualization (lead); Writing – original draft (supporting); Writing – review & editing (lead).

DATA AVAILABILITY

The data that support the findings of this study are available within the article.

APPENDIX A: FORMATION OF NECK IN THE CASE WITH FIXED ω

For radiation with fixed frequency ω , let us find the condition for the formation of a neck between forbidden regions. Functions b_{\pm} in the case with fixed ω are

$$b_{\pm} = \frac{1}{f}(-2au \pm \sqrt{\Delta}), \quad \Delta = (1 - q^2 f \mathcal{R}) \mathcal{D}r^2. \quad (\text{A1})$$

As mentioned in Sec. III, this is just the first expression in (9) with \mathcal{D} multiplied by $1 - f\zeta^2$ (since $\zeta^2 = q^2\mathcal{R}$). Function $\hat{\mathcal{R}} = f\mathcal{R}$ appearing in the definition of Δ can be written as

$$\hat{\mathcal{R}} \propto (1 - 2u)u^2 / (1 + r_c^2 u^2).$$

The function is positive for $0 < u < 1/2$, it vanishes at both $u = 0$ and $u = 1/2$, and its derivative, $d\hat{\mathcal{R}}/du \propto 1 - 3u - r_c^2 u^3$, decreases monotonically with u , crossing zero at some $u_C < 1/2$. Thus, $\hat{\mathcal{R}}$ has the maximum at $r_C = u_C^{-1} > 2$. Denote $q_{\text{crit}} = \hat{\mathcal{R}}_C^{-1/2}$. For $q = q_{\text{crit}}$, the curves b_+ and b_- merge at r_C ; in fact, they develop spikes directed against each other, whose tips touch at r_C . The reason is that in the vicinity of $r = r_C$ the function Δ is proportional to δ^2 , where $\delta = r - r_C$, so that functions b_{\pm} assume the form $b_{\pm} = A + B\delta \pm C|\delta|$, and as a result, have spike-like minimum and maximum at $\delta = 0$. For $q > q_{\text{crit}}$, Δ becomes negative in some interval (r_A, r_B) containing r_C , the larger the greater the value of q ; therefore, the two regions inaccessible for rays become connected by a neck that extends from r_A to r_B . For the parameters used in Fig. 2 we have $r_C = 3.104$, which yields $\hat{\mathcal{R}}_C = 0.1418$ and $q_{\text{crit}} = 2.656$. Note that the interval (r_A, r_B) lies entirely above $r = 2$ for any $q > q_{\text{crit}}$ since $\Delta = (1 + |f|\zeta^2)\mathcal{D}r^2 > 0$ for $r < 2$. For $q = 3.5$ (the value used in the right panel of Fig. 2), the neck extends from $r_A = 2.268$ to $r_B = 5.727$.

APPENDIX B: ALLOWED REGIONS FAR FROM THE HORIZON AND CLOSE TO IT IN THE CASE WITH FIXED ω_0

For radiation with fixed frequency ω_0 seen by a LNRF observer, function F determining allowed regions has the form $F = k + 2lb + mb^2$, where coefficients k, l, m can be expressed in terms of function $Q = q\Gamma_0\sqrt{\mathcal{D}}Rr$ as

$$k = \mathcal{A}r^2 - Q^2, \quad l = -2au + Q^2\Omega_0, \quad m = -f - Q^2\Omega_0^2. \quad (\text{B1})$$

Solutions to equation $F = 0$ are $b_{\pm} = -(l \pm \sqrt{\Delta})/m$, where $\Delta = l^2 - km$.

For $r \gg 1$, Q approaches the value $Q_{\infty} = q\Gamma_0 r_{0+}$, where $r_+ = (r^2 + r_c^2)^{1/2}$; hence, F can be written as $F \doteq r^2 + 2Q_{\infty}^2\Omega_0 b - (1 + Q_{\infty}^2\Omega_0^2)b^2$ and the solutions to the equation $F = 0$ in the leading order in r are $b_{\pm} = \pm Cr$, where $C = (1 + Q_{\infty}^2\Omega_0^2)^{-1/2}$. Since $C < 1$, the wedge-like band between the forbidden regions narrows down if we fix ω_0 instead of ω .

In order to determine the behavior of constant C as a function of r_0 , let us express constant $\hat{q} = Q_{\infty}\Omega_0$ appearing in the definition of C as

$$\hat{q} \propto r_{0+}u_0^3 / \sqrt{\mathcal{A}_0\mathcal{D}_0} = r_{0+} / (\sqrt{r_0 A_0 D_0}),$$

where $A = \mathcal{A}r^3 = r^3 + a^2 r + 2a^2$ and $D = \mathcal{D}r^2 = r^2 - 2r + a^2$. The expression for \hat{q} can be written as a product of functions r_+/r , $\sqrt{r/A}$ and $1/\sqrt{D}$, evaluated at $r = r_0$; and since function r_+/r obviously decreases with r for all $r > 0$, while functions A/r and D can be shown to increase with r for $r > r_h$, constant \hat{q} decreases and constant $C = (1 + \hat{q}^2)^{-1/2}$ increases as r_0 goes from r_h to ∞ . The former constant decreases from ∞ to 0 for r_0 increasing from r_h to ∞ , hence, the latter constant increases from 0 to 1. For the parameters used in Fig. 3 we have $C = 0.681$ (left panel) and 0.9997 (right part of the right panel).

Consider now the radius r_a at which either b_- or b_+ has an asymptote. The value of r_a is given by the equation $m_a = -f_a - Q_a^2\Omega_0^2 = 0$, i.e., $f_a = -\hat{q}^2 D_a / r_{a+}^2$ (since $Q = Q_{\infty}\sqrt{D}/r_+$). Function f is negative only for $r < 2$ so that the asymptote lies necessarily there; and since it is located at $r = 2$ in case with fixed ω , the inner borderline of forbidden regions, or region in case with a neck, shifts towards r_h as we fix ω_0 instead of ω .

Function $-f$ falls from a positive value to 0 as r rises from r_h to 2, while function D/r_+^2 can be shown to rise from 0 to a positive value. Thus, the asymptote is the closer to the static limit the smaller the value of \hat{q} ; and since \hat{q} falls from ∞ to 0 as r_0 rises from r_h to ∞ , the asymptote shifts with increasing r_0 from r_h to 2. For the parameters used in Fig. 3 we have $r_a = 1.836$ (left panel) and 1.691 (the left part of right panel).

For radiation with fixed ω we had $r_a = 2$ and the divergent function was b_- , just as in case without plasma. Now we have $r_a < 2$ and the divergent function may be b_+ , too: it is b_- if $l_a < 0$ and b_+ if $l_a > 0$. In the latter case, forbidden regions are necessarily connected with a neck and the way their boundary approaches the asymptote at $r = r_a$ is reversed as compared with the former case: function b_+ is falling to $-\infty$ to the left of the asymptote and rising to $+\infty$ to the right. Let us write $l_a = -2au_a - f_a/\Omega_0 \propto \lambda_a - 1$, where $\lambda = -f/(2a\Omega_0 u) = A_0(2 - r)/(4a^2)$. As r rises from r_h to 2, λ falls linearly from $\lambda_h = A_0 r_{h-}/(4a^2)$ to 0, where r_{h-} is the radius of the inner horizon, $r_{h-} = 1 - \sqrt{1 - a^2}$ (the smaller root of $\mathcal{D} = 0$). It can be easily proven that $\lambda_h > 1$, so that $\lambda > 1$ below some radius $r_1 > r_h$; explicitly, $r_1 = r_h + r_{h-}(1 - 1/\lambda_h)$. For the parameters used in the left part of the right panel of Fig. 3 we have $r_1 = 1.625 < r_a = 1.691$; thus, the function diverging at r_a is b_- . Note that in order that the diverging function is b_+ , the parameter q needs to satisfy $q > q_{\text{rev}} = (\Gamma_0\Omega_0)^{-1}\sqrt{-f_1/(D_1\mathcal{R}_1)}$ (“rev” stands for “reversed”). In our case $q_{\text{rev}} = 1.421$, so that $q < q_{\text{rev}}$.

APPENDIX C: FORMATION OF NECK IN CASE WITH FIXED ω_0

In the case radiation has fixed frequency ω_0 with respect to a LNRF observer, the discriminant of equation $F = 0$ is

$$\Delta = (1 - q^2\Gamma_0^2 f_+ \mathcal{R})\mathcal{D}r^2, \quad f_+ = f + 4ar^{-1}\Omega_0 - \mathcal{A}r^2\Omega_0^2. \quad (\text{C1})$$

If forbidden regions in the (r, b) -plane are connected by a neck, the radii r_A and r_B , where the inner edge of the neck is farthest from the horizon and the outer edge is closest to it, are given by the equation $X = 0$, where $X = 1 - q^2 \Gamma_0^2 f_+ \mathcal{R}$ is the extra factor by which Δ differs from $\hat{\Delta} = \mathcal{D}r^2$ [see Eq. (C1)]. While in case with fixed ω the neck forms only for large enough q , now it can exist for arbitrary q , provided r_0 lies outside a certain interval (ρ_{0A}, ρ_{0B}) . To see that, consider asymptotics of X for $r_0 \sim r_h$ and $r_0 \gg 1$.

Close to the horizon, at $\varepsilon = r - r_h \ll 1$, we have $\mathcal{D} \doteq 2\sqrt{1 - a^2 u_h^2} \varepsilon \equiv u_h^2 \hat{\varepsilon}$, and the value of function \mathcal{A} at the horizon is $\mathcal{A}_h = 4u_h^2$. Thus, if the observer is shifted with respect to the horizon by $\varepsilon_0 \ll 1$, their Γ -factor is $\Gamma_0 \doteq (\mathcal{A}_h / \mathcal{D}_0)^{1/2} \doteq 2\hat{\varepsilon}_0^{-1/2}$; furthermore, for the angular velocity of the observer we have $\Omega_0 \doteq \Omega_h = \frac{1}{2} a u_h$. As seen from these expressions, function X reduces close to the horizon to $X \doteq 1 - 4q^2 \hat{\varepsilon}_0^{-1} f_+$, where $r f_+ = r - 2 + 4a\Omega_0(1 - \frac{1}{4} a^{-1} A\Omega_0) \doteq r - 2 + 2a^2 u_h(1 - \frac{1}{8} u_h A) \doteq [1 - \frac{1}{4} a^2(3 + a^2 u_h^2)] \varepsilon \equiv C\varepsilon$. (We have used the fact that if r_0 as well as r are $\sim r_h$, then $\mathcal{R} \doteq 1$.) As a result, for $\varepsilon_0 \ll 1$ there exists a neck in the (r, b) -plane with the inner edge bent away from the horizon up to $\varepsilon_A = \frac{1}{4} q^{-2} (r_h / C) \hat{\varepsilon}_0$. If we denote $\alpha = \sqrt{1 - a^2}$, we have $\hat{\varepsilon}_0 = 2\alpha\varepsilon_0$ and $4r_h^2 C = (4 - 3a^2)r_h^2 - a^4 = 2\alpha r_h^3$ (as seen by writing r_h as $1 + \alpha$); hence, $\varepsilon_A = q^{-2} \varepsilon_0$. Note that from the expansion of F up to the first order in ε it follows that the asymptote of b_- is shifted with respect to the horizon by the same value, $\varepsilon_a = q^{-2} \varepsilon_0$. Thus, if we want to check that $\varepsilon_A > \varepsilon_a$ (the point where b_- merges with b_+ lies beyond the asymptote of either b_- or b_+), we need to proceed to the next-to-leading order in ε_0 .

In the opposite limit, when $r_0 \gg 1$, we have $\Gamma_0 \doteq 1$ and $\Omega_0 = O(u_0^3)$; if, moreover, $r \sim r_0$, we have also $f_+ \doteq 1$ and $\mathcal{R} \doteq r_0^2 u^2$. Thus, the asymptotics of function X far from the horizon is $X \doteq 1 - q^2 r_0^2 u^2$; and, consequently, there exists a neck in the (r, b) -plane with the outer edge bent towards the horizon down to $r_B = qr_0$.

The values of r_0 for which the neck shrinks to a point, along with the values of r where the point is located, are given by equations $X = X' = 0$. The first equation is just $q^2 \Gamma_0^2 f_+ \mathcal{R} = 1$, while the second equation can be written as a cubic equation for $u = r^{-1}$,

$$(f_+ \mathcal{R})' \propto (1 - a\Omega_0)^2 u(3 + r_c^2 u^2) - (r_c^2 - a^2)\Omega_0^2 - 1 = 0.$$

If we express u as function of Ω_0 by Cardano's formula and solve equation $X = 0$ with this u inserted into it numerically, we obtain two pairs of values (r_0, r) . For the parameters used in Fig. 4 these values are $(\rho_{0A}, \rho_A) = (1.726, 2.176)$ and $(\rho_{0B}, \rho_B) = (6.769, 3.080)$. As seen from our analysis of the limit cases $r_0 \sim r_h$ and $r_0 \gg 1$, forbidden regions develop a neck for $r_0 < \rho_{0A}$ as well as for $r_0 > \rho_{0B}$; hence, for r_0 from the interval (ρ_{0A}, ρ_{0B}) they are necessarily separated by a free band. Moreover, the fact that the interval (ρ_A, ρ_B) lies entirely inside the interval (ρ_{0A}, ρ_{0B}) suggests that the inequalities $\varepsilon_A = q^{-2} \varepsilon_0 > \varepsilon_0$ and $r_B = qr_0 < r_0$, obtained in the limits $r_0 \sim r_h$ and $r_0 \gg 1$, stay valid all the way from $r_0 = r_h$ up to $r_0 = \rho_{0A}$ and from $r_0 = \infty$ down to $r_0 = \rho_{0B}$. This is easily verified numerically, because equation $X = 0$ is cubic in r , therefore we can once again use Cardano's formula to express its solutions, radii r_A and r_B , analytically as functions of r_0 .

APPENDIX D: CONSTRUCTING ALLOWED REGIONS IN THE (r_0, b) -PLANE

Let us find functions $B_{\pm} = b_{\pm}(r_0)$ for a LNRF observer. Define $\mathcal{F} = Fu^2 = \hat{\mathcal{F}} - \mathcal{D}\zeta^2$, where $\hat{\mathcal{F}} = \hat{F}u^2 = \mathcal{A} - 4au^3b - fu^2b^2$ and ζ is given by Eq. (10). If we rewrite $\hat{\mathcal{F}}$ as $\hat{\mathcal{F}} = \mathcal{A}(1 - \Omega b)^2 - \mathcal{D}u^2b^2/\mathcal{A}$, we obtain $\hat{\mathcal{F}}_0 = \mathcal{A}_0\kappa_0^2 - \mathcal{D}_0u_0^2b^2/\mathcal{A}_0$, where $\kappa_0 = 1 - \Omega_0b$. [The expression for $\hat{\mathcal{F}}$ which we have started from follows immediately from the identity $f\mathcal{A} + 4a^2u^4 = \mathcal{D}$, but it can also be obtained by rewriting the 2D metric as $ds_2^2 = -\mathcal{D}dt^2/\mathcal{A} + \mathcal{A}r^2d\tilde{\phi}^2$, where $d\tilde{\phi} = d\phi - \Omega dt$, and by regarding the formula $\hat{\mathcal{F}} = -\omega^{-2}\mathcal{D}g^{AB}\tilde{k}_A\tilde{k}_B$ with $\tilde{k}_A = \omega(-1 + \Omega b, b)$.] Since $\zeta_0^2 = q^2\Gamma_0^2\kappa_0^2 = q^2\mathcal{A}_0\kappa_0^2/\mathcal{D}_0$, we find $\mathcal{F}_0 = (1 - q^2)\mathcal{A}_0\kappa_0^2 - \mathcal{D}_0u_0^2b^2/\mathcal{A}_0 \propto \hat{\mathcal{F}}_0(\mathcal{D}_0 \rightarrow \mathcal{D}_0/(1 - q^2))$, and by putting this expression equal to zero we obtain

$$B_{\pm} = \frac{\mathcal{A}_0r_0^2}{2ar_0^{-1} \pm \sqrt{\mathcal{D}_0/(1 - q^2)}}. \tag{D1}$$

Functions B_{\pm} have the asymptotics $B_{\pm} = \pm\sqrt{1 - q^2}r_0$ for $r_0 \gg 1$. Furthermore, the asymptotics of \mathcal{F}_0 for $b \rightarrow \pm\infty$ is $\mathcal{F}_0 = [(1 - q^2)\mathcal{A}_0\Omega_0^2 - \mathcal{D}_0u_0^2/\mathcal{A}_0]b^2 \propto [1 - q^2 - \mathcal{D}_0r_0^4/(4a^2)]b^2$; hence, the radius r_{0a} at which function B_- has an asymptote is given by $\sqrt{\mathcal{D}_{0a}r_{0a}^2/(2a)} = \sqrt{1 - q^2}$. For the parameters used in Fig. 4 we have $r_{0a} = 1.874$.

For any given r_0 from the interval (ρ_{0A}, ρ_{0B}) we can find the impact parameters B_{\pm} at the lowest point of the upper forbidden corner and at the highest point of the lower forbidden corner in the (r, b) -plane, and by repeating this procedure for a sequence of nearby r_0 's covering the interval (ρ_{0A}, ρ_{0B}) we can construct the lines \mathcal{B}_{\pm} in the (r_0, b) -plane. The line \mathcal{B}_- lies under the line \mathcal{B}_+ inside the interval (ρ_{0A}, ρ_{0B}) and merges with it at the end points of the interval; therefore, the two lines form a loop in the (r_0, b) -plane. In region \mathcal{O}_{h+i} inside the loop, rays can reach observers from both sides, from the horizon as well as from infinity, while at the boundary of \mathcal{O}_{h+i} (the line $\partial\mathcal{O}_{h+i}$ composed of \mathcal{B}_+ and \mathcal{B}_-) the rays arrive at the observers from one side only, either from the horizon or from infinity. Let us discuss the position of the points P_{\pm} separating the two parts of the $\partial\mathcal{O}_{h+i}$ with opposite directions of the incoming light, and the behavior of the lines B_{\pm} and \mathcal{B}_{\pm} in their neighborhood.

As r_0 rises from ρ_{0A} to ρ_{0B} , the radii R_+ and R_- , at which function b_+ has minimum (radius R_+) and function b_- has maximum (radius R_-), change from ρ_A to ρ_B : the radius R_+ first rises and then falls, while the radius R_- first falls and then rises. Since $\rho_A > \rho_{0A}$ and $\rho_B < \rho_{0B}$, both radii necessarily equal r_0 at some point, the radius R_+ at $r_0 = R_{0+}$ and the radius R_- at $r_0 = R_{0-}$. By the definition of points P_{\pm} , the radii $R_{0\pm}$ are the values of the radius r_0 at which these points are located in the (r_0, b) -plane. Obviously, functions $B_+(r_0)$ and $B_+(r_0)$ coincide at $r_0 = R_{0+}$,

and functions $B_-(r_0)$ and $B_+(r_0)$ coincide at $r_0 = R_{0-}$. The radii $r = R_{\pm}$ are given by equation $\partial_r b_{\pm}(r_0, r) = 0$ or, equivalently, by equation $\partial_r F(r_0, r, b)|_{b=b_{\pm}(r_0, r)} = 0$. Thus, for radii $r_0 = R_{0\pm}$ we have equation $\partial_r F(r_0, r_0, b)|_{b=B_{\pm}(r_0)} = 0$. To put this into a compact form, introduce new variables $x = fb + 2au$ and $y = 1 - \Omega_0 b$ and write functions F and $\partial_r F$ as $fF = D - x^2 - fQ^2 y^2$ and $\partial_r(fF) \propto \frac{1}{2} \mu - (x - \frac{1}{2}a)^2 - \frac{1}{2} f \dot{Q}^2 y^2$, where $Q^2 = q^2 \Gamma_0^2 D \mathcal{R}$, $\mu = \frac{1}{2}(fD'r^2 + a^2) = r^3 - 3r^2 + 2r + \frac{1}{2}a^2$ and $\dot{Q}^2 = \frac{1}{2}r^2(fQ^2)'$ and $v = r^3 - 2r^2 + a^2 - fDr^3/r_+^2$. By combining equations $F(r_0, r_0, b) = 0$ (definition of B_{\pm}) and $\partial_r F(r_0, r_0, b) = 0$, we obtain

$$\Phi_{\pm} \equiv \frac{1}{2}\mu_0 - (X_{\pm} - \frac{1}{2}a)^2 - \frac{1}{2}v_0(1 - X_{\pm}^2/D_0) = 0, \tag{D2}$$

where $X_{\pm} = x_0(B_{\pm}) = f_0 B_{\pm} + 2au_0$. The desired radii are found by solving equations $\Phi_{\pm} = 0$ for r_0 ; for the parameters used in Fig. 4 the radii are $R_{0+} = 1.965$ and $R_{0-} = 3.593$.

Points P_{\pm} are not just common points of lines \mathcal{B}_{\pm} and B_{\pm} ; they are *points of the tangency* of those lines. This is clear from the very fact that there is just one common point for each pair of lines, but it can be seen also from the behavior of functions $B_{\pm}(r_0)$ and $B_{\pm}(r_0)$ close to $R_{0\pm}$. Consider functions with index $+$. Since $B_+(r_0)$ is the minimum of function $b_+(r_0, r)$, there must hold $B_+ > \mathcal{B}_+$ in the neighborhood of R_{0+} ; however, this can be satisfied for $r_0 > R_{0+}$ only if $dB_+/dr_0 \geq d\mathcal{B}_+/dr_0$ at R_{0+} , and for $r_0 < R_{0+}$ only if $dB_+/dr_0 \leq d\mathcal{B}_+/dr_0$ at R_{0+} . Thus, the derivatives of B_+ and \mathcal{B}_+ coincide at R_{0+} .

Equation $\Phi_{\pm} = 0$ has, in addition to solutions $r_0 = R_{0\pm}$ depending on parameters a, r_c and q , also solution $r_0 = 2$ valid for all values of parameters. Indeed, for $r_0 = 2$ we have $\mu_0 = \frac{1}{2}a^2$, $X_{\pm} = a$ and $D_0 = a^2$, so that $\Phi_{\pm} = \frac{1}{4}a^2 - (a - \frac{1}{2}a)^2 = 0$. However, this does not mean that the radii R_{\pm} merge with r_0 twice, once at the static limit, provided it falls into the interval (ρ_{0A}, ρ_{0B}) , and once outside it. The reason is that the coefficient of proportionality in the expression for $\partial_r F$ contains factor f^{-2} , so that the equation to be solved is actually $f_0^{-2} \Phi_{\pm} = 0$; and since for $r_0 \sim 2$ it holds $f_0 = \varepsilon_0/2$ and $\Phi_{\pm} = O(\varepsilon_0^2)$, where $\varepsilon_0 = r_0 - 2$, the equation is in the generic case *not* solved by $r_0 = 2$. If we introduce constants $k_{\pm} = (p \mp 1)/(p \pm 1)$, where $p = 1/\sqrt{1 - q^2}$, and denote $l = 2/r_+(2) = 2/(4 + r_c^2)^{1/2}$, we can write the coefficients in $\Phi_{\pm} = K_{\pm} \varepsilon_0^2$ as

$$K_{\pm} = -(1 + \frac{1}{2}a^2) \left[2(1 + \frac{1}{2}a^2)a^{-2}q^{-2} - l^2 - \frac{1}{2} \right] k_{\pm} + \frac{3}{2} + \frac{1}{8}a^2.$$

The coefficients are both $\propto -a^{-2}$ for $a \sim 0$, and as a rises to 1, K_- stays negative, while K_+ crosses 0 at some $a_{\text{crit}} < 1$, provided q is not too close to 1. If parameters r_c and q are such as in Fig. 4, $r_c = 1$ and $q = 2/3$, the critical value of a is $a_{\text{crit}} = 0.784$. From the behavior of functions Φ_{\pm} at $r_0 = r_h$ and $r_0 \gg 1$ it follows that they cross 0 at $r_0 > 2$ if they touch the r_0 axis from below at $r_0 = 2$, and at $r_0 < 2$ if they touch the r_0 axis from above. Thus, $R_{0-} > 2$ for all a 's and $R_{0+} > 2$ for $a < a_{\text{crit}}$, but $R_{0+} < 2$ for $a > a_{\text{crit}}$. The value of a used in Fig. 4 is a bit greater than a_{crit} , that is why point P_+ is shifted a bit to the left of $r_0 = 2$.

The derivatives of B_{\pm} and \mathcal{B}_{\pm} at $r_0 = R_{0\pm}$ are proportional to the function

$$(\partial_r F)_0 = -2Q_0^2 Y, \quad Y = [(r_0 - a^2 u_0^2)r_0/A_0 - (r_0 - 1)/D_0 + r_0/r_{0+}^2]y + 2a(3r_0^2 + a^2)b/A_0^2,$$

evaluated at $b = B_{\pm}$. The derivatives seem to be zero in Fig. 4, but in fact they are only *almost* zero. To see this, compare the radii $R_{0\pm}$ to the radii $\hat{R}_{0\pm}$ at which $Y = 0$: for the parameters used in Fig. 4 it holds $\hat{R}_{0+} = 1.944$ and $\hat{R}_{0-} = 3.580$; hence, \hat{R}_{0+} is close to R_{0+} and \hat{R}_{0-} is close to R_{0-} . By combining the expression for $(\partial_r F)_0$ given above with the formula $\partial_b F_0 = -2(x_0 - Q_0^2 \Omega_0 y)$, we find that $d\mathcal{B}/dr_0 = -0.0794$ at $r_0 = R_{0+}$ and $d\mathcal{B}/dr_0 = 0.0074$ at $r_0 = R_{0-}$.

APPENDIX E: ALLOWED REGIONS FOR FREELY FALLING OBSERVERS

We are interested in allowed regions in the (r_0, b) -plane for rays seen by freely falling observers. Function $\mathcal{F} = Fu^2$ determining these regions has again, as in the problem with LNRF observers analyzed in Appendix D, the form $\mathcal{F} = \tilde{\mathcal{F}} - \mathcal{D}\zeta^2$; however, ζ is now given by Eq. (11). Let us write the additional term appearing in \mathcal{F} due to the presence of plasma as $\mathcal{D}\zeta^2 = \gamma(\kappa_0 - \xi_0 \eta_0)^2$, where $\kappa_0 = 1 - \Omega_0 b$ and $\gamma = q^2 \hat{\Gamma}_0^2 \mathcal{D}\mathcal{R}$. (If we wrote function \mathcal{F} for a LNRF observer as quadratic polynomial in b , in the coefficients there would appear instead of function Q^2 , function $Q^2 = Q^2 u^2 = q^2 \Gamma_0^2 \mathcal{D}\mathcal{R}$. Since γ is obtained from this function by replacing $\Gamma_0 \rightarrow \hat{\Gamma}_0$, we can write it as $\gamma = \hat{Q}^2$.) To make formulas describing radiation seen by the two classes of observers more similar to each other, define an "effective LNRF parameter" $q_{\text{NR}} = q \hat{\Gamma}_0 / \Gamma_0 = q \Gamma_0$; then, $\gamma = q_{\text{NR}}^2 \Gamma_0^2 \mathcal{D}\mathcal{R}$ and $\gamma_0 = q_{\text{NR}}^2 \mathcal{A}_0$.

A new feature of the theory in the case with freely falling observers is the identity $\mathcal{F}_0 = \eta_0^2$. The difference between the two sides of the equation can be written as the polynomial $K_0 + 2L_0 \eta_0 + M_0 \eta_0^2$, where

$$K_0 = -\tilde{\mathcal{F}}_0 + \gamma_0 \kappa_0^2, \quad L_0 = -\gamma_0 \xi_0 \kappa_0, \quad M_0 = 1 + \gamma_0 \xi_0^2. \tag{E1}$$

The polynomial has two roots $\eta_0^{(\pm)} = (-L_0 \pm \sqrt{\delta_0})/M_0$, where $\delta_0 = L_0^2 - K_0 M_0$. Note that the coefficient in front of η_0^2 can be written as $M_0 = 1 + q_{\text{NR}}^2 (1 - \Gamma_0^{-2})$.

By plugging expressions for K_0 , L_0 , M_0 into the definition of δ_0 we find $\delta_0 = M_0 \dot{\mathcal{F}}_0 - \gamma_0 \kappa_0^2$. If we define a “modified effective LNRF parameter” $\tilde{q}_{\text{NR}} = M_0^{-1/2} q_{\text{NR}}$ and introduce functions $\tilde{\gamma} = \tilde{q}_{\text{NR}}^2 \Gamma_0^2 \mathcal{O}R$ and $\tilde{\mathcal{F}}_{\text{NR}} = \dot{\mathcal{F}} - \tilde{\gamma} \kappa_0^2$, we can write $\delta_0 \propto \tilde{\mathcal{F}}_{\text{NR},0}$; thus, rays can reach the observer at $r = r_0$ with the desired frequency only if $\tilde{\mathcal{F}}_{\text{NR},0} \geq 0$. From the analysis of allowed regions in the (r_0, b) -plane for LNRF observers (see Appendix D) we know that parameter \tilde{q}_{NR} must be < 1 in order that there exists a non-empty class of rays that arrive at the observer with the desired frequency, and the rays must have b from the interval(s) delimited by functions $\tilde{B}_\pm = B_\pm(q \rightarrow \tilde{q}_{\text{NR}})$ [see Eq. (D1)], in order that they fall into that class. Which rays are allowed depends on whether r_0 is greater or less than radius \tilde{r}_{0a} at which function \tilde{B}_- has an asymptote: for $r_0 > \tilde{r}_{0a}$ the rays must have $\tilde{B}_- < b < \tilde{B}_+$, while for $r_0 < \tilde{r}_{0a}$ they need to have either $b < \tilde{B}_+$ or $b > \tilde{B}_-$. Thus, similarly to the problem with LNRF observers, there are two distinct allowed regions in the (r_0, b) -plane: region $\tilde{\mathcal{O}}_I$ extended over all r_0 's, with $\tilde{B}_- < b < \tilde{B}_+$ for $r_0 > \tilde{r}_{0a}$ and $b < \tilde{B}_+$ for $r_0 < \tilde{r}_{0a}$; and region $\tilde{\mathcal{O}}_{II}$ extended over the interval $r_0 < \tilde{r}_{0a}$ only, with $b > \tilde{B}_-$.

At the boundaries of regions $\tilde{\mathcal{O}}_I$ and $\tilde{\mathcal{O}}_{II}$ rays do not have turning points as in the problem with LNRF observers; instead, they have a nonzero rescaled radial velocity η_0 there, $\eta_0 < 0$ at $\partial\tilde{\mathcal{O}}_I$ and $\eta_0 > 0$ at $\partial\tilde{\mathcal{O}}_{II}$. Inside regions $\tilde{\mathcal{O}}_I$ and $\tilde{\mathcal{O}}_{II}$ we have two values of η_0 assigned to each point, one ($\eta_0^{(-)}$ in $\tilde{\mathcal{O}}_I$ and $\eta_0^{(+)}$ in $\tilde{\mathcal{O}}_{II}$) with the same sign as η_0 at the boundary of the region and another ($\eta_0^{(+)}$ in $\tilde{\mathcal{O}}_I$ and $\eta_0^{(-)}$ in $\tilde{\mathcal{O}}_{II}$) with opposite sign in a smaller region. In the latter case, the sign of η_0 changes at lines B_\pm given by equation $\mathcal{F}_{\text{NR},0} = 0$, where $\mathcal{F}_{\text{NR}} = \dot{\mathcal{F}} - \gamma \kappa_0^2$.

As r_0 decreases from ∞ to r_h , Γ_0 increases from 1 to ∞ , and as a result, \tilde{q}_{NR} increases for the given $q < 1$ from q to 1 (since $\tilde{q}_{\text{NR}} = q_{\text{NR}}/[1 + q_{\text{NR}}^2(1 - \Gamma_0^{-2})]^{1/2} = q/[(1 - q^2)\Gamma_0^{-2} + q^2]^{1/2}$). If the value of q is fixed, the form of regions $\tilde{\mathcal{O}}_I$ and $\tilde{\mathcal{O}}_{II}$ changes substantially in the vicinity of the horizon in comparison with what we have obtained for LNRF observers: rather than merge at $b = b_h$ on the horizon, the regions become separated by a gap between $b_{h\pm} = b_h/[1 \pm (1 - q^2)^{-1/2} q b_h]$. For the parameters used in Fig. 5, $b_{h+} = 1.045$ and $b_{h-} = -2.188$. (Thus, the gap lays entirely under the merging point at $b_h = 4$.) If we want to preserve the form of regions $\tilde{\mathcal{O}}_I$ and $\tilde{\mathcal{O}}_{II}$ as they look in the problem with LNRF observers, we need to fix \tilde{q}_{NR} rather than q ; for r_0 decreasing from ∞ to r_h we will then have q decreasing from \tilde{q}_{NR} to 0 (since $q = \tilde{q}_{\text{NR}}/[(1 - \tilde{q}_{\text{NR}}^2)\Gamma_0^2 + \tilde{q}_{\text{NR}}^2]^{1/2}$). Note that q_{NR} increases with decreasing r_0 from \tilde{q}_{NR} to $\tilde{q}_{\text{NR}}/(1 - \tilde{q}_{\text{NR}}^2)^{1/2}$, which is > 1 if $\tilde{q}_{\text{NR}} > 1/\sqrt{2}$. For such \tilde{q}_{NR} the constant q_{NR} surpasses 1 at some $r_{0,\text{lim}} > r_h$, which means that functions B_\pm are defined only for $r_0 \geq r_{0,\text{lim}}$ – there is no change of sign of η_0 between r_h and $r_{0,\text{lim}}$. For the value $\tilde{q}_{\text{NR}} = 2/3$ used in Fig. 5, functions B_\pm are defined for all values of r_0 .

We want to determine the lines dividing the (r_0, b) -plane into regions \mathcal{O}_{h+i} , \mathcal{O}'_h and \mathcal{O}'_i . For LNRF observers, we did it by computing functions \mathcal{B}_\pm , equal for each r_0 to the value of b at the lowest point of the upper forbidden corner and at the highest point of the lower forbidden corner in the (r, b) -plane. Calculation of \mathcal{B}_\pm was straightforward, since equation $\mathcal{F}(r, r_0, b) = 0$ for the boundaries of the corners, lines $b_\pm(r, r_0)$, was quadratic, and hence could be solved analytically. Now we have two classes of rays with different values of η_0 – class I with $\eta_0 = \eta_0^{(+)}$ and class II with $\eta_0 = \eta_0^{(-)}$, so we have also two functions \mathcal{F} ,

$$\mathcal{F}^{(\pm)} = \mathcal{F}(\eta_0 = \eta_0^{(\pm)}) = \dot{\mathcal{F}} - \tilde{\gamma}(M_0^{-1} N_0 \kappa_0^2 + \xi_0^2 \dot{\mathcal{F}}_0 \mp 2\xi_0 M_0^{-1/2} \dot{\mathcal{F}}_{\text{NR},0}^{1/2} \kappa_0), \quad (\text{E2})$$

where $N_0 = 1 - \gamma_0 \xi_0^2 = 1 - q_{\text{NR}}^2(1 - \Gamma_0^{-2})$. Values of b satisfying equations $\mathcal{F}^{(\pm)} = 0$ are now solutions to *quartic* equation $\mathcal{F}^{(+)} \mathcal{F}^{(-)} = 0$. Even though there exists analytical solution in this case, too, it is not too practical to determine functions \mathcal{B}_\pm from it. Instead, we can compute \mathcal{B}_\pm for both $\eta_0^{(+)}$ and $\eta_0^{(-)}$ by looking for the values of b for which the minimum of $\mathcal{F}^{(+)}$ and $\mathcal{F}^{(-)}$ crosses zero (which may or may not happen for given r_0).

The lines we are searching for were, in the problem with LNRF observers, just two parts of the boundary of region \mathcal{O}_{h+i} , separated by points P_\pm . Now they are still parts of that boundary, but they are separated by finite segments of lines \tilde{B}_\pm rather than by points lying on them. At the endpoints of these segments, points P_{A+} and P_{B+} on the line \tilde{B}_+ and points P_{A-} and P_{B-} on the line \tilde{B}_- , there are rays whose value of b is either maximum (in points P_{A+} , P_{B+}) or minimum (in points P_{A-} , P_{B-}) among all rays coming to the observer with the desired frequency. Rays in points $P_{A\pm}$ arrive from and rays in points $P_{B\pm}$ head for the peak of the forbidden region in the (r, b) -plane. Thus, radial coordinates of the peaks, radii $R_{A\pm}$ and $R_{B\pm}$, differ from radial coordinates of the observers, radii $R_{0A\pm}$ and $R_{0B\pm}$: radii $R_{A\pm}$ are greater than $R_{0A\pm}$ and radii $R_{B\pm}$ are less than $R_{0B\pm}$. For the parameters used in Fig. 5, we have $(R_{0A+}, R_{A+}) = (1.708, 1.900)$, $(R_{0B+}, R_{B+}) = (2.405, 1.919)$, $(R_{0A-}, R_{A-}) = (2.859, 3.644)$ and $(R_{0B-}, R_{B-}) = (4.548, 3.624)$.

Line $\mathcal{B}_+^{(+)}$ lying on the border of the upper part of region $\mathcal{O}_{h+i}^{(+)}$, adjacent to the arc $P_{A+}P_{B+}$, line $\mathcal{B}_-^{(+)}$ forming the boundary of the lower part of region $\mathcal{O}_{h+i}^{(+)}$, adjacent to the arc $P_{A-}P_{B-}$, as well as lines $\mathcal{B}_\pm^{(-)}$ demarcating region $\mathcal{O}_{h+i}^{(-)}$, are all tangent to the boundaries of region $\tilde{\mathcal{O}}_I$, lines $\mathcal{B}_+^{(+)}$ to \tilde{B}_+ and lines $\mathcal{B}_-^{(+)}$ to \tilde{B}_- , just as in the problem with LNRF observers lines \mathcal{B}_\pm were tangent to lines B_\pm . To see why, consider lines in the vicinity of point P_{B+} . In the vertical band of the diagram for rays of class I, where the boundary of region \mathcal{O}_{h+i} crosses the lines $r_0 = \text{const}$ three times, we have, in addition to forbidden corner, a separate forbidden region in (r, b) -plane bounded from both sides in the form of a slant cigar. Rays with $b = \tilde{B}_+$ on the right of the point P_{B+} , at $r_0 > R_{0B+}$, bounce back from the lower edge of a forbidden corner after passing by the observer, while those on the left of the point P_{B+} , at $r_0 < R_{0B+}$, hit the upper edge of a forbidden cigar. This leads, just as in the problem with LNRF observers, to inequalities $d\mathcal{B}_+/dr_0 \geq d\mathcal{B}_+^{(-)}/dr_0$ for $r_0 \rightarrow R_{0B+}^+$ and $d\mathcal{B}_+/dr_0 \leq d\mathcal{B}_+^{(+)}/dr_0$ for $r_0 \rightarrow R_{0B+}^-$. The difference is that now for r_0 passing through R_{0B+} from values $> R_{0B+}$, forbidden corner first shrinks to a point and then stretches to a forbidden cigar, while before, as r_0 passed through R_{0+} , forbidden corner just shifted to the left without changing its form. However, numerical calculation suggests that the transformation from a corner to a cigar, even though it seems discontinuous, is smooth enough to preserve the value of $d\mathcal{B}_+/dr_0$.

In the problem with freely falling observers, regions \mathcal{O}_{h+i} for rays of classes I and II look significantly different, each in its own way, from region \mathcal{O}_{h+i} in the problem with LNRF observers. It is not only that, as we just discussed, they are attached to forbidden regions at finite segments of their boundaries rather than touching them at a single point; region \mathcal{O}_{h+i} also shrinks to a point at a pair of points Q_{\pm} lying on the lines B_{\pm} for rays of class I, and it is attached to the horizon in a finite interval of values of b for rays of class II.

As seen in Fig. 5, the boundary of $\mathcal{O}_{h+i}^{(-)}$ consists of two parts, broken arcs $P_{A+}P_{A-}$ and $P_{B+}P_{B-}$ intersecting at points Q_{\pm} . The intersection at Q_{-} has the form of a “straight cross,” the cross at Q_{+} is “inclined” (the detailed numerics shows that in fact the arc $P_{B+}P_{B-}$ at Q_{+} is first deflected slightly to the left and only then turns sharply to the right). In the vicinity of point Q_{-} there are two forbidden regions in the (r, b) -plane, a cigar and an upper corner in a finite height above it, and as r_0 passes through the radial coordinate of point Q_{-} , $r_{Q-} = 3.494$, the cigar shrinks to a point and then stretches again, leaning to the other side than before. To the right of point Q_{+} , there is a cigar and a lower corner which approach each other as r_0 passes through the radial coordinate of point Q_{+} , $r_{Q+} = 2.159$, and at $r_0 < r_{Q+}$ only the corner remains. Since the left boundary of the central part of region $\mathcal{O}_{h+i}^{(+)}$ turns to the right under the point Q_{+} , minimum radii (r_0, r) in that region are just $\rho_{0A}^{(+)} = \rho_A^{(+)} = r_{Q+}$. For maximum radii numerical calculation yields $(\rho_{0B}^{(+)}, \rho_B^{(+)}) = (3.966, 3.161)$.

The endpoints of the interval of b where region $\mathcal{O}_{h+i}^{(-)}$ is attached to the horizon coincide with impact parameters $\hat{b}_{ph\pm}$ of photon orbits in vacuum. To see that, express additional term in \mathcal{F} due to the presence of plasma as $\Delta\mathcal{F} = -k_0^2\mathcal{D}\mathcal{R}$, where $k_0 = q_{NR}\Gamma_0\tilde{\kappa}_0$ and $\tilde{\kappa}_0 = \kappa_0 - \xi_0\eta_0$, write the factor $\tilde{\kappa}_0$ for rays of class II as $\tilde{\kappa}_0 = \kappa_0 - \xi_0(-L_0 - \sqrt{\delta_0})/M_0 = [\kappa_0 + \xi_0(M_0\tilde{\mathcal{F}}_{NR,0})^{1/2}]/M_0$, insert into the expression under the square root $\tilde{\mathcal{F}}_{NR,0} = \tilde{\mathcal{F}}_0 - \tilde{\gamma}_0\kappa_0^2 = (1 - \tilde{q}_{NR}^2)\mathcal{A}_0\kappa_0^2 - \mathcal{D}_0u_0^2b^2/\mathcal{A}_0$ (this is just the expression for \mathcal{F}_0 obtained at the beginning of Appendix D, with q replaced by \tilde{q}_{NR}) and take the limit $r_0 \rightarrow r_h$. It holds $\xi_h = -\mathcal{A}_h^{-1/2}$, $M_h = 1 + q_{NR}^2 = 1/(1 - \tilde{q}_{NR,h}^2)^{1/2}$ (since $q_{NR,h} = (q_0\Gamma_0)(r_0 \rightarrow r_h) = \tilde{q}_{NR}/(1 - \tilde{q}_{NR}^2)^{1/2}$) and $\tilde{\mathcal{F}}_{NR,h} = (1 - \tilde{q}_{NR}^2)\mathcal{A}_h$, so that $\tilde{\kappa}_h \propto \kappa_h - |\kappa_h| = 0$ (since $\kappa_h > 0$ for $b = \hat{b}_{ph\pm}$). Thus, for $\varepsilon_0 = r_0/r_h \ll 1$ we have $\tilde{\kappa}_0 = O(\varepsilon_0)$, and since $\Gamma_0 = O(\varepsilon_0^{-1/2})$, we have also $k_0 = O(\varepsilon_0^{1/2})$ and $k_h = 0$. We see that function $\mathcal{F}(r, r_0, b)$ reduces to $\tilde{\mathcal{F}}(r, b)$ at $r_0 = r_h$; therefore, functions $B_{\pm}(r_0)$, defined by equations $\mathcal{F}(r, r_0, b) = \partial_r\mathcal{F}(r, r_0, b) = 0$, reduce to $\hat{b}_{ph\pm}$ at $r_0 = r_h$. For Kerr parameter $a = 0.8$ used in Fig. 5, this yields extreme values of b for rays seen by an observer on the horizon (in the sense of limit) $(\mathcal{B}_{h+}, \mathcal{B}_{h-}) = (3.237, -6.662)$. Finally, since region $\mathcal{O}_{h+i}^{(-)}$ is adjacent to the horizon, the radii from which radiation has access to the black hole are bounded only from above: for the parameters used in Fig. 5, maximum radii (r_0, r) are $(\rho_{0B}^{(-)}, \rho_B^{(-)}) = (11.378, 3.067)$.

REFERENCES

- ¹J. Renn and T. Sauer, “Eclipses of the stars—Mandl, Einstein, and the early history of gravitational lensing,” in *Revisiting the Foundations of Relativistic Physics: Festschrift in Honour of John Stachel*, edited by A. Ashtekar, R. Cohen, D. Howard *et al.* (Kluwer Academic Publishers, Dordrecht, 2003), pp. 69–92.
- ²P. Schneider, J. Ehlers, and E. Falco, *Gravitational Lensing* (Springer-Verlag, Berlin, 1992).
- ³V. Perlick, *Ray Optics, Fermat’s Principle, and Applications to General Relativity* (Springer, Berlin, 2000).
- ⁴J. Wambsganss, *Living Rev. Relativ.* **1**, 12 (1998).
- ⁵R. D. Blandford and C. S. Kochanek, “Gravitational lenses,” in *Dark Matter in the Universe: Proceedings of the 117th Symposium of the International Astronomical Union Held in Princeton, NJ, June 24–28, 1985*, edited by J. Kormendy and G. R. Knapp (Springer, Dordrecht, 1987), pp. 133–195.
- ⁶F. De Felice, *Nuovo Cimento B* **57**, 351 (1968).
- ⁷S. E. Vazquez and E. P. Esteban, *Nuovo Cimento B* **119**(5), 489 (2004).
- ⁸S. E. Gralla and A. Lupsasca, *Phys. Rev. D* **101**(4), 044031 (2020).
- ⁹S. V. Iyer and E. C. Hansen, *Phys. Rev. D* **80**(12), 124023 (2009).
- ¹⁰J. M. Bardeen, “Timelike and null geodesics in the Kerr metric,” in *Black Holes*, edited by C. DeWitt and B. DeWitt (Gordon & Breach, New York, 1973), p. 215.
- ¹¹O. Semerák, *Helv. Phys. Acta* **69**(1), 69 (1996).
- ¹²J. Schee, Z. Stuchlík, and J. Juráň, “Light escape cones and raytracing in Kerr geometry,” in *RAGtime 6/7: Workshops on Black Holes and Neutron Stars*, edited by S. Hledík (Silesian University, Opava, 2005), pp. 143–155.
- ¹³K. Ogasawara and T. Igata, *Phys. Rev. D* **103**(4), 044029 (2021).
- ¹⁴V. Perlick and O. Y. Tsupko, *Phys. Rev. D* **95**(10), 104003 (2017).
- ¹⁵M. Fathi, M. Olivares, and J. R. Villanueva, *Eur. Phys. J. C* **81**(11), 987 (2021).
- ¹⁶A. Chowdhuri and A. Bhattacharyya, *Phys. Rev. D* **104**(6), 064039 (2021).
- ¹⁷J. L. Synge, *Relativity: The General Theory* (North-Holland Publishing Company, Amsterdam, 1960).
- ¹⁸J. Bičák and P. Hadrava, *Astron. Astrophys.* **44**(2), 389 (1975).
- ¹⁹G. S. Bisnovaty-Kogan and O. Yu. Tsupko, *Gravitation Cosmol.* **15**(1), 20 (2009).
- ²⁰O. Y. Tsupko and G. S. Bisnovaty-Kogan, *Phys. Rev. D* **87**(12), 124009 (2013).
- ²¹G. S. Bisnovaty-Kogan and O. Yu. Tsupko, *Universe* **3**(3), 57 (2017).
- ²²O. Y. Tsupko, *Phys. Rev. D* **103**(10), 104019 (2021).
- ²³B. Bezděková, V. Perlick, and J. Bičák, *J. Math. Phys.* **63**(9), 092501 (2022).
- ²⁴T. Kimpson, K. Wu, and S. Zane, *Mon. Not. R. Astron. Soc.* **484**(2), 2411 (2019).
- ²⁵M. Sárényi and V. Balek, *Gen. Relativ. Gravitation* **51**(11), 141 (2019).
- ²⁶G. Hinshaw and L. M. Krauss, *Astrophys. J.* **320**(2), 468 (1987).
- ²⁷X. Er and S. Mao, *Mon. Not. R. Astron. Soc.* **437**(3), 2180 (2014).

²⁸G. S. Bisnovatyi-Kogan and O. Y. Tsupko, *Mon. Not. R. Astron. Soc.* **404**(4), 1700 (2010).

²⁹I. D. Novikov and K. S. Thorne, "Astrophysics of black holes," in *Black Holes*, edited by C. DeWitt and B. DeWitt (Gordon & Breach, New York, 1973), pp. 343–450.

³⁰C. Liu, C. Ding, and J. Jing, *Chin. Phys. Lett.* **34**(9), 090401 (2017).

³¹J. Bičák and Z. Stuchlík, *Mon. Not. R. Astron. Soc.* **175**(2), 381 (1976).

³²C. W. Misner, K. S. Thorne, and J. A. Wheeler, *Gravitation* (W. H. Freeman & Co., San Francisco, 1973).